THE ASTROPHYSICAL JOURNAL, 471:254–278, 1996 November 1

EXTREMELY METAL-POOR STARS. II. ELEMENTAL ABUNDANCES AND THE EARLY CHEMICAL ENRICHMENT OF THE GALAXY[1]

SEAN G. RYAN
Anglo-Australian Observatory, P.O. Box 296, Epping, NSW 2121, Australia, and National Astronomical Observatory, 2-21-1 Osawa, Mitaka, Tokyo 181, Japan; sgr@aaoepp.aao.gov.au

JOHN E. NORRIS
Mount Stromlo and Siding Spring Observatories, Australian National University, Private Bag, Weston Creek Post Office, ACT 2611, Australia; jen@mso.anu.edu.au

AND

TIMOTHY C. BEERS
Department of Physics and Astronomy, Michigan State University, East Lansing, MI 48824; beers@pa.msu.edu
Received 1996 April 19; accepted 1996 June 4

ABSTRACT

We have obtained high-resolution spectra of 23 very metal-poor stars and present an abundance analysis for 19 of these for elements between Mg and Eu. The sample comprises roughly equal numbers of dwarfs and giants. All stars have [Fe/H] < -2.5, and 10 have [Fe/H] < -3.0. In addition, for six stars with [Fe/H] < -3.0, we compile equivalent widths from the literature (including our own studies) and recompute abundances. Possible errors in the stellar atmospheric models are discussed in detail. Hyperfine-structure corrections are presented for Mn and Co. We use robust techniques to delineate the main trends in the [X/Fe] versus [Fe/H] plots and compare these with the Galactic chemical evolution computations of Timmes, Woosley, & Weaver.

The main results are as follows: The lowest abundance we derive for a previously unobserved star is [Fe/H] $= -3.57$, for CS 22172−002. There are now six stars with [Fe/H] < -3.50 as determined from high-resolution analyses. The α-elements Mg, Si, Ca, and Ti possess almost uniform overabundances (relative to iron) down to at least [Fe/H] $= -4$, the current limit of observations. [Mg/Fe] increases slightly at [Fe/H] < -2.5, but the slope is only -0.15 dex dex^{-1} and may be due to systematic errors. Ti behaves like the other α-elements, contrary to stellar nucleosynthetic calculations. Stars with [Fe/H] < -2.5 reach a plateau in [Al/Fe] $\simeq -0.8$ that extends at least down to [Fe/H] $= -4$, but Baumueller & Gehren have advised of the need for $+0.5$ dex non-LTE corrections in the dwarfs, leading to a revised plateau nearer [Al/Fe] $\simeq -0.3$. This level is qualitatively consistent with an odd-even effect for Mg and Al, and in quantitative agreement with Timmes et al.'s Galactic chemical evolution model. We confirm the underabundance of [Cr/Fe] and [Mn/Fe], and the overabundance of [Co/Fe], in stars with [Fe/H] < -2.5 that was highlighted by McWilliam et al. In addition, we point to a mild overabundance in [Ni/Fe], though this may be dominated by a few stars that have higher than normal [Ni/Fe] but that do not reflect an overall trend. Like CS 22949−037, discussed by McWilliam et al., CS 22876−032 shows real variations in yields, with Al and Mg produced in their normal ratios to one another but with underabundances in [Si/Fe], [Ca/Fe], and possibly [Sc/Fe]. It is clear from several elements that real star-to-star abundance differences are common at the lowest metallicities. Sr is measured in most of our stars, but Y and Ba are generally strong enough only in the giants. [Sr/Fe] shows a spread greater than 2 dex (i.e., by a factor in excess of 100) at [Fe/H] < -3, greatly exceeding reasonable errors in the measurement. This spread exists for both dwarfs and giants. [Ba/Fe] decreases as [Fe/H] falls below -2.0, and it exhibits less scatter than [Sr/Fe]. A small number of stars with [Ba/Fe] > 0 deserve further study. CS 22897−008 has high Sr, Y, and C abundances for its [Fe/H] but normal Ba. This signature may have arisen from the weak *s*-process in $M > 15\ M_\odot$ stars or by *r*-processing.

By combining an analytic description of gaseous supernova remnants with supernova yields, we show that enrichment of the interstellar medium is influenced more by supernova physics (explosive energy) than by environmental conditions (cloud density). If supernova iron-peak yields are correlated with explosion energy, we can accommodate the well-defined abundance trends with a chaotic picture for halo formation involving independently evolving clouds, as was envisaged by Searle & Zinn. We calculate that a typical enrichment in the protohalo will produce [Fe/H] $= -2.7$. This coincides with larger abundance variations in field stars of lower metallicity and the lower abundance limit for Galactic globular clusters.

Subject headings: Galaxy: formation — nuclear reactions, nucleosynthesis, abundances — stars: abundances — stars: Population II — subdwarfs

[1] Based on observations obtained with the University College London echelle spectrograph at the 3.9 m Anglo-Australian Telescope, and the Australian National University 2.3 m telescope.

1. INTRODUCTION

Extremely metal-poor stars exhibit the products of nucleosynthesis from the first high-mass, zero-metallicity objects to evolve and pollute the proto-Galaxy. Elemental abundance ratios observed in the low-mass stars that survive to the present allow us to probe the ejecta of these earliest supernovae and determine the nature of the stars and sites of nucleosynthesis that existed during the first epochs of star formation in the Galaxy.

The changing elemental abundance ratios observed at different metallicities can be compared with the yields computed for supernovae of different masses to determine which have contributed to Galactic chemical enrichment and when. The observed abundances also feed back into nucleosynthetic calculations when unexpected elemental ratios are found, constraining efforts to produce more realistic supernova models.

Elemental abundance ratios at $[Fe/H] \gtrsim -2.5$ were reviewed extensively in the late 1980s (e.g., Lambert 1989; Wheeler, Sneden, & Truran 1989). The main trends for halo stars at that time could be summarized as follows: the α-elements (Mg, Si, Ca, and Ti) were essentially uniformly overabundant relative to Fe by 0.3–0.4 dex. Oxygen behaved similarly, though it was controversial at the time whether the overabundance was uniform or increased with decreasing iron abundance. Aluminum became more underabundant relative to iron at lower metallicities, suggesting that its production was linked to the existing metallicity of the stellar material. Most iron-group elements tracked the iron abundance, with the notable exception of Mn, the underabundance of which mirrored the overabundance of the α-elements. The neutron-capture elements showed a range of behaviors, but broadly speaking, Sr tracked Fe whereas the heavier element Ba became underabundant at $[Fe/H] < -2$. Gilroy et al. (1988) showed, however, that real star-to-star differences existed for heavy elements among metal-poor stars, indicating that the protohalo was not well mixed when these stars formed.

Since the late 1980s, the data at $-4 < [Fe/H] < -3$ have increased significantly. Many of these stars were identified in objective-prism searches for extremely metal-poor stars (Beers, Preston, & Shectman 1985, 1992b) and in a study of proper-motion stars (Ryan, Norris, & Bessell 1991). Halo stars with $[Fe/H] > -2.5$ tend to have similar elemental abundance ratios (with the exception of Al and the neutron-capture elements); the more metal-deficient stars do not. The spread in neutron-capture elements becomes even greater at lower metallicities (Ryan et al. 1991; Norris, Peterson, & Beers 1993; Sneden et al. 1994; McWilliam et al. 1995a), and large overabundances in C have been detected in many stars (Beers et al. 1992b; McWilliam et al. 1995a). The lack of consistent behavior among stars of the same iron abundance emphasizes that the star-forming environment during the early stages of halo formation was not well mixed. Furthermore, the large variations we see at very low metallicities probably reflect shot noise from the small numbers of supernovae effecting the enrichment.

A recent unexpected find was that iron-group abundances change considerably in going to $[Fe/H] < -2.5$ (McWilliam et al. 1995a). The atomic mass distribution of nuclei shifts toward higher atomic masses at lower metallicities and must reflect changing conditions in the supernovae responsible. (The nuclei affected are produced deep in the supernova, close to the mass cut.) McWilliam et al. suggested a possible process (the α-rich freezeout); supernova-yield computations have yet to predict this abundance signature in detail.

In order to study these and other effects in more detail, we sought to discover and analyze larger numbers of extremely metal-poor stars, with particular interest in those having $[Fe/H] < -3.0$. In this work, we analyze high-resolution spectra of 22 stars, 10 of which have $[Fe/H] < -3.0$. The study is part of a much larger investigation of extremely metal-deficient stars; Beers, Norris, & Ryan (1996) provide details on the full observational program. In Paper I of the present series (Norris, Ryan, & Beers 1996a), we presented equivalent widths from high-resolution blue spectra of 23 stars. In the present paper, we analyze these data, deriving elemental abundances and discussing their interpretation. In § 2, we provide a brief summary of the steps that led to the isolation of the sample that we discuss here. The abundance analysis is described in § 3, and in § 4 we compare our results with other studies in the cases of overlap. The resulting chemical abundances are discussed in § 5.

The terms "iron abundance" and "metallicity" are often used interchangeably, but they cannot always be treated thus. In contrast to the old, metal-deficient stars of the Galactic halo, whose chemical compositions were shaped by preceding generations of stars and which form the topic of the present study, there exist stars with extremely low abundances of certain elements as a result of phenomena associated with events during their own lifetimes. Van Winckel, Waelkens, & Waters (1995) have discussed a class of post–asymptotic giant branch (AGB) stars in binary orbits that are deficient in iron and some other elements by even greater factors than the Galactic halo stars studied here, down to $[Fe/H] = -4.8$. However, these stars have normal surface abundances for many other elements and are explained by way of a circumstellar shell in which the least volatile atomic species condense onto grains that are blown away from the star by radiation pressure during the AGB phase. The cleaned gas is later reaccreted onto the star, aided by the binary configuration.

A different class of iron-poor, chemically peculiar stars is that of the "CH subgiants" (Bond 1974), enriched in carbon and *s*-process elements. Bond suggested that these might be "reevolving" stars that had mixed excessively during a former AGB phase. McClure (1984) found a very high incidence of binaries among CH stars and, drawing parallels with the Population I barium stars, noted the probable importance of the binary nature in generating the peculiar abundances, though it was unclear whether this was due to the now evolved companion having dumped AGB-processed material onto the subgiant companion or whether the binary nature somehow triggered excessive mixing of the style discussed by Bond. A related object is G77−61, a dwarf with very low metal abundances but a carbon abundance ~1/10 of solar (Gass, Liebert, & Wehrse 1988). Beers et al. (1985, 1992b) discovered several very metal-poor stars with strong CH features. One is included in our sample, along with two others we discovered in a separate investigation of high–proper motion stars. Because their chemical compositions may reflect more their dangerous liaisons than the evolution of the Galaxy, we have deferred discussion of these cases to a separate paper (Norris, Ryan, & Beers 1996c).

2. SELECTION, OBSERVATION, AND BASIC DATA OF PROGRAM STARS

The extremely metal-poor stars taken from the literature included those already identified by Beers et al. (1985, 1992b), the *r*-process star CS 22892−052, drawn to our attention by Sneden et al. (1994), two possibly similar stars—LP 706−7 and LP 625−44—identified by Ryan & Norris (1991a), and G186−26, known for its severe Li deficiency (Hobbs, Welty, & Thorburn 1991). Three other stars from the literature, G108−33 (Carney et al. 1994), HD 122563, and HD 140283, were also included. In addition, we have undertaken our own discovery program (described below) among objective prism–selected stars; objects contributed by that study make up almost half of the sample under discussion. Supplementary data on these stars may be found in Beers et al. (1996). Equivalent width measurements from high-resolution blue echelle spectra for 23 stars were presented in Paper I.

The broader observing program to identify new extremely metal-poor stars from objective-prism data is detailed by Beers et al. (1996), and only a short summary will be given here. Following procedures established by Beers et al. (1985), T. C. B. has continued an objective-prism survey of many fields in the northern and southern hemispheres, visually scanning the plates (aided by a 10× microscope) to identify weak-lined candidates. J. E. N. and S. G. R. obtained *UBV* photometry of many of the southern candidates to identify those that show the ultraviolet excess expected of metal-deficient stars, followed by 1 Å resolution spectroscopy at the Ca II K line of the more promising cases. Stars with [Fe/H] $\lesssim -3$, as inferred from the Ca II K line (Beers, Flynn, & Gebhardt 1990a), were placed on the list for observation at high resolution.

We defer discussion of the stars with very strong CH features to Paper IV (Norris et al. 1996c). We intend this as a *morphological* division of the sample since it would be premature to assign some astrophysical cause to these unusual abundances prior to undertaking a detailed study. However, in light of the considerable spectral differences between the stars CS 22892−052, LP 625−44, and LP 706−7, on the one hand, and the remainder of our sample on the other, separation seemed reasonable. The Li-weak star G186−26 is discussed in Paper III (Norris, Ryan, & Beers 1996b).

The stars analyzed in this paper are listed in Table 1. The first 19 utilize solely our own spectroscopic data and are grouped according to evolutionary type. The signal-to-

TABLE 1

BASIC DATA FOR PROGRAM STARS

Star	Type[a]	S/N	$B-V$	$E(B-V)$	$R-I$	$T_{\rm eff}$ (K)	ϵ_T (K)	log g[b]	[Fe/H]	ζ[c] (km s^{-1})	$n_{\rm Fe\,I}$	$\sigma_{\rm Fe\,I}$	$\epsilon_{\rm Fe\,I}$	Notes
Based on Equivalent Widths Measured by Norris et al. (1996a, Table 1)														
CD −38°245	G	40	0.81	0.00	0.505	4850	30	1.5s	−3.96	2.4	69	0.22	0.09	
CS 22897−008	G	39	0.76	0.00	0.511	4850	30	1.8s	−3.19	1.7	95	0.25	0.09	
CS 22952−015	G	48	0.79	0.02	0.515	4850	40	1.6s	−3.31	2.5	104	0.19	0.09	
CS 22172−002[d]	G	50	0.81	0.06	0.544	4900	80	1.8s	−3.57	2.2	88	0.26	0.12	
HD 122563	G	110	0.91	0.00	0.56	4650	30	1.4s	−2.68	2.6	165	0.21	0.09	
CS 22186−005	HB	35	0.38	0.00	0.308	6000	50	2.0s	−2.77	3.2	58	0.23	0.10	$v \sin i = 9 \pm 1$ km s^{-1}
BS 16547−049[d]	SG	53	0.50	0.07	0.373	5850	150	3.0s	−3.01	1.4	67	0.22	0.17	
CS 22943−137	SG	40	0.47	0.00	0.362	5650	50	3.5e	−3.22	1.3	58	0.22	0.10	
CS 30308−062[d]	SG	42	0.40	0.00	0.318	5950	50	3.6s	−2.92	1.0	55	0.18	0.10	
HD 140283	SG	232	0.49	0.01	...	5750	50	3.4s	−2.54	1.4	153	0.13	0.10	
BS 16472−070[d]	TO	53	0.42	0.05	0.309	6300	110	3.9s	−2.71	1.5	65	0.19	0.14	
BS 16968−061[d]	TO	48	0.43	0.02	0.320	6000	60	4.0e	−3.08	1.5	64	0.18	0.11	
CS 22166−030[d]	TO	41	0.45	0.01	0.349	5800	50	4.0e	−3.36	1.0	47	0.23	0.10	=CS31065−008
CS 22171−016[d,e]	TO	47	0.40	0.00	0.303	6100	50	2.5s	−3.3	1.0	19	0.21	0.11	1.0*W*
								2.5s	−2.9	1.7	19	0.24	0.11	1.5*W*
CS 22953−037	TO	54	0.39	0.00[f]	0.292	6150	50	4.0e	−2.94	1.2	56	0.18	0.10	
CS 29491−084[d]	TO	40	0.38	0.00	0.290	6200	50	4.0e	−2.74	1.2:	57	0.24	0.10	
CS 29499−060	TO	39	0.38	0.00	0.288	6200	50	4.0s	−2.63	1.0	65	0.25	0.10	
CS 29527−015[d]	TO	28	0.40	0.00	0.292	6150	50	4.0e	−3.43	1.3:	14	0.16	0.11	
G108−33	TO	33	0.44	0.03	0.316	6100	80	4.0e	−2.69	1.0:	47	0.23	0.12	
Based on Compilation by Norris et al. (1996a, Table 2)														
CS 22876−032	TO	...	0.40	0.01	0.31	6100	50	4.0e	−3.85	1.5	35	0.12	0.10	1, 2
CS 22885−096	G	...	0.69	0.03	0.48	5050	50	2.0s	−3.60	1.8	96	0.30	0.10	2, 3, 4
CS 22897−008	G	...	0.76	0.00	0.511	4850	30	1.8s	−3.34	2.0	144	0.25	0.09	4, 5
CS 22952−015	G	...	0.79	0.02	0.515	4850	40	1.4s	−3.26	2.5	143	0.20	0.09	4, 5
CS 22968−014	G	...	0.73	0.02	0.50	4950	40	1.8s	−3.43	2.3	130	0.27	0.10	2, 4, 6
CD −38°245	G	...	0.81	0.00	0.505	4850	30	2.0s	−3.92	2.1	109	0.22	0.09	1, 4, 5, 6, 7, 8, 9

[a] G = giant, HB = horizontal branch, SG = subgiant, TO = main-sequence turnoff.

[b] Suffixes indicate gravities based on spectroscopic ionization balance ("s") or evolutionary status ("e").

[c] Suffix ":" indicates assumed microturbulence because analysis was poorly constrained.

[d] Newly identified metal-poor star from Beers et al. 1996.

[e] CS 22171−016, a double-lined spectroscopic binary, was analyzed under two limiting cases in which the observed equivalent widths of the primary were (1) taken at face value and (2) multiplied by 1.5 to compensate for the continuum contribution of the secondary; see § 3.4.3.

[f] Schuster et al. 1996 give $E(b-y) = 0.056$. A reddening this large would imply an effective temperature ∼400 K higher and an iron abundance ∼0.3 dex higher.

REFERENCES.—(1) Molaro & Castelli 1990; (2) Norris et al. 1993; (3) Molaro & Bonifacio 1990; (4) McWilliam et al. 1995a; (5) this paper; (6) Primas et al. 1994; (7) Bessell & Norris 1984; (8) Gratton & Sneden 1988; (9) Peterson et al. 1990.

noise ratio (S/N) varies throughout each echelle spectrum: in the table, we provide the S/N per 0.04 Å pixel at 4300 Å; we refer the reader to Paper I for discussion of random and systematic errors in the equivalent widths. The $B-V$ and $R-I$ photometry comes primarily from our measurements at the 2.3 m telescope on Siding Spring Mountain (Norris, Ryan, & Beers 1996d) but includes data from Carney et al. (1994) for G108−33, from Bessell & Norris (1984) for CD −38°245 and HD 122563, and from Gratton & Sneden (1991) for the last of these. If not included in these references, reddening estimates are based on reddening maps, following Ryan (1989).

In Paper I, we compiled an extended line list for six very metal-poor stars, combining various equivalent width measurements from the literature (including our new observations). This reduces random errors in equivalent widths and provides additional lines, which is important for poorly represented atomic species. These factors also permit an improved determination of the surface gravity and microturbulence. These six stars are listed at the end of Table 1. For the three that do not appear in our own spectroscopy program, we adopt the photometric colors listed by Norris et al. (1993, Table 3).

3. ABUNDANCE ANALYSIS

Utilizing the equivalent width measurements from Paper I, one may compute an LTE abundance for a spectral line by using Kurucz's WIDTH6 program once the following information is available: (1) the effective temperature, surface gravity, and metallicity for the stars, (2) a model atmosphere with those parameters, and (3) atomic data for the spectral line. We discuss each of these in the following subsections.

3.1. *Atmospheric Parameters*

We assumed initially that stars identified from the objective-prism survey were either at the main-sequence turnoff or more evolved. Dereddened $B-V$ and $R-I$ colors [adopting $E(R-I) = 0.7E(B-V)$] were transformed to effective temperatures by use of calibrations based on atmospheric models. For dwarfs and subgiants, we adopted $B-V$ and $R-I$ versus $T_{\rm eff}$ transformations from Bell & Oke (1986) and Buser & Kurucz (1992), applying the 0.02 mag offset recommended by Bell & Oke for their own $R-I$ calibration. For the giants, the $B-V$ and $R-I$ calibrations of Bell & Gustafsson (1978, 1989, respectively) were adopted. Since $R-I$ is less dependent on metallicity than $B-V$, temperatures from the former were given twice the weight.

Errors in the adopted effective temperatures arise from random photometric errors (typically $\sim$0.01 in $B-V$ and $R-I$), from the estimated reddening, which may be in error by on order of half its value,[2] and from systematic errors in the adopted color–effective temperature transformations, which could easily be in error by up to 100 K (and by different amounts for different evolutionary classes). We adopt a random component of 0.01 mag in each color, corresponding to 25 K in $B-V$ and 50 K in $R-I$ in the giants and to 40 K in $B-V$ and 85 K in $R-I$ in the turnoff stars, and an additional uncertainty of $0.5E(B-V)$, which we combine in quadrature. The error estimates so obtained are included in Table 1 as ϵ_T; these ignore possible systematic revisions of the color–effective temperature transformations, which may or may not be metallicity dependent.

Turnoff stars were initially assumed to have surface gravities of $\log g = 4.0$, subgiants $\log g = 3.5$, and giants $\log g = 2.0$. If more than one or two Fe II lines were measured, the gravities were revised during the analysis to establish the Fe I–to–Fe II ionization balance. The final values are listed in Table 1, where an appended letter indicates whether the gravity was derived spectroscopically ("s") or was based on the assumed evolutionary status ("e").

3.2. *Model Atmospheres*

Not all grids of model atmospheres yield identical structures for a requested effective temperature, surface gravity, and metallicity. We discuss two specific differences that may affect abundance computations.

3.2.1. *Temperature Gradient through the Line-forming Region*

Differences in the handling of convection can affect the transfer of energy through the atmosphere and therefore change the temperature gradient in the outer layers. One such difference exists between old (R. L. Kurucz 1989, private communication) and new Kurucz (1993) models, the later set having temperatures up to 200 K hotter in the line-forming regions than older models of the same $T_{\rm eff}$/log g/[Fe/H]. For the stars in our program, Fe I abundances computed by using the newer models would be higher since a larger abundance is required to reproduce a given equivalent width.

The difference between the old and new Kurucz models came to our attention when we tried unsuccessfully to reproduce in detail the abundances published by Norris et al. (1993), which had been computed using Kurucz's more recent atmospheres. We, on the other hand, used models from R. A. Bell (1983, private communication) and Bell et al. (1976), and from Kurucz (1989, private communication) that we had previously found to be in good agreement with Bell's models for overlapping ranges of $T_{\rm eff}$/log g/[Fe/H]. Our models yielded Fe I abundances lower by 0.1 dex at the main-sequence turnoff and lower by 0.15 dex on the giant branch. These differences were traced to the differences in temperature structure noted above, which Bell (1994, private communication) suspects are due to the differences in convection. Other elements and ionization states will also be affected, to differing degrees depending on their sensitivity to temperature.

In the present work, we have adopted the models from Bell and colleagues since these cover the parameter range of our stars and are more directly comparable with models used in most previous studies.

3.2.2. *The Outermost Layers*

Although an abundance analysis would preferably be carried out with weak lines having $\log (W_\lambda/\lambda) \lesssim -5$, for some elements stronger spectral features have to be used. McWilliam et al. (1995a) have reported that for (violet) lines stronger than 85–100 mÅ, the Bell models can reach significant optical depth in the first tabulated layer, meaning that significant line formation is occurring above the tabulated atmosphere.

A second effect discussed by McWilliam et al. is the influence of a chromosphere, which reverses the outward decline of temperature, resulting in a minimum around

[2] Regrettably, the zero point may also be in error; see Schuster et al. (1996).

(0.75–0.80)$T_{\rm eff}$. McWilliam et al. overlaid scaled empirical chromospheres onto their photospheres and found, again, that lines stronger than 85–100 mÅ were affected. Errors of order 0.1 dex were introduced in strong-line abundances through the neglect of a chromosphere.

Following our own investigation of the Bell models, we do not believe we are fully exposed to all of the concerns expressed by McWilliam et al. Two examples illustrate our reasons. In their Figure 7, McWilliam et al. compare Kurucz theoretical models and JILA empirical models of Arcturus. Whereas they note that the Bell models do not extend to sufficiently distant layers, we find that our model of Arcturus (using $T_{\rm eff}$/log g/[Fe/H] = 4300/1.7/−0.5) has its second level at the same column mass (RHOX) as the JILA temperature minimum and that the temperature in this Bell layer matches the Kurucz value. Given the great uncertainty in the models beyond the temperature minimum and the shallow depth at which this occurs, we could not be convinced to favor the Kurucz model over the Bell one. Second, in their discussion of BD −18°5550, McWilliam et al. report that the Bell et al. models begin at RHOX $\sim$ 13 g cm^{-2}. However, the closest model we have to this star (admittedly at a higher gravity, log g = 1.5, though this should not matter greatly) has its second layer at RHOX = 2.2 g cm^{-1}, considerably further out than McWilliam et al. found.

For additional warnings on the validity of models in the outermost layers, we refer the interested reader to the discussion in Gustafsson et al. (1975).

3.2.3. *Let the Buyer Beware!*

The concern expressed by McWilliam et al. followed their discovery of differences of $\lesssim$0.1 dex in the abundances derived from Kurucz models and from Bell et al. models, particularly for lines stronger than $\sim$100 mÅ. We have found greater similarity between the two sets of models and conclude that we will be susceptible to smaller errors than those discussed by McWilliam et al. and that the differences that remain will be systematic. However, as noted in § 3.2.1, we do identify other differences between the newest Kurucz grid and the Bell grids, associated with the temperature gradient. The bottom line is clear: *the limitations of the stellar atmospheric models must be borne in mind in any discussion of stellar abundances.* Systematic differences of $\lesssim$0.1 dex can be found between studies that utilize different grids of model atmospheres.

3.3. *Atomic Parameters and Solar Abundances*

An error in the log *gf* of a transition appears directly in the derived abundance for a line, so we examine log *gf*–values in detail below. Damping constants, on the other hand, are of importance only in strong lines, which we do not deal with here. We note for completeness that we enhanced Unsöld's (1955) treatment of van der Waal's broadening by a factor of 2.2 (in γ), but this will not affect our conclusions based on weak lines.

Our intention was to proceed with an absolute abundance analysis in LTE utilizing laboratory oscillator strengths (where possible) rather than solar *gf*-values since the lines are very much stronger in the Sun than in our stars, and consequently the solar *gf*-values would be sensitive to the treatment of damping in the solar analysis. However, in the final step of the abundance analysis, we subtract the solar abundance to express our result in the traditional form [A/B] $\equiv$ log $(N(\mathrm{A})/N(\mathrm{B}))_*$ − log $(N(\mathrm{A})/N(\mathrm{B}))_\odot$, so it is important that the adopted solar abundance is consistent with the *gf*-scale. The log *gf*–values are tabulated in Paper I, but specific notes for some elements are made below. Except as noted, we have adopted the solar photospheric abundances given by Anders & Grevesse (1989). One important exception is iron, for which we adopted a lower value, which we discuss first. Notes on a subset of the other elements follow.

3.3.1. *Iron*

Fe I.—The high-precision absorption work of the Oxford group (Blackwell, Petford, & Shallis 1979b; Blackwell et al. 1979a, 1980, 1982a; Blackwell, Petford, & Simmons 1982b), and more recently the emission data of O'Brian et al. (1991) (which appear to be in good agreement), have provided log *gf*–values accurate to a few times 0.01 dex. However, there is ongoing debate over the solar abundance. The Oxford group (including Blackwell, Lynas-Gray, & Smith 1995 and Blackwell, Smith, & Lynas-Gray 1995) maintain a "high" value,[3] log N(Fe) = 7.63, whereas Holweger et al. (1991; Holweger, Kock, & Bard 1995) obtained log N(Fe) = 7.48 (LTE; 7.51 non-LTE). A recent "third party," Kostik, Shchukina, & Rutten (1996), derived 7.62 but concluded that the debate remains open. Clearly, the absolute iron abundance of the brightest star is still unknown. This uncertainty affects the zero point of our Fe abundance scale but not the star-to-star differences. We adopt the value 7.50, which also agrees with the meteoritic abundance (7.51, Anders & Grevesse 1989). We adopt *gf*-values from the Oxford group, O'Brian et al., Bard, Kock, & Kock (1991), and Bard & Kock (1994) as our first preference and, otherwise, accept values from the Fuhr, Martin, & Wiese (1988) compilation or other sources if necessary. As Table 1A of Paper I shows, more than 90% of the *gf*-values come from the preferred sources.

Fe II.—Experimental values come from a number of sources. Most recent analyses lead to solar abundances close to 7.50, and NLTE corrections appear to be negligible, as expected for this dominant ionization state (7.48, Holweger, Heise, & Kock 1990; 7.54, Biémont et al. 1991; 7.48, Hannaford et al. 1992).

3.3.2. *Other Elements*

Magnesium.—The solar photospheric Mg abundance, 7.58 (Anders & Grevesse 1989), which matches the meteoritic value, is based on the analysis of Lambert & Luck (1978), who, measuring 7.59 for Mg I, utilized theoretical *gf*-values from Froese Fischer (1975). We follow their lead in using her values where possible. We have measurements of up to eight Mg I lines, but we mostly rely on those at 3829 and 4703 Å. For half of our lines, and in particular the 3829 Å transition, theoretical *gf*-values are not available and we are forced to utilize solar *gf*-values. Lines common to Thévenin (1989) and Froese Fisher suggest that values of log *gf* for the former should be increased by 0.28 dex, but the adjusted Thévenin *gf* that we used for the 4571Å line then yielded abundances systematically lower than the Froese Fisher lines in our program stars by roughly the same amount. Consequently, we utilized the 4571 Å log *gf*

[3] On a scale where log N(H) = 12.00.

of Thévenin unchanged, viz., −5.61.[4] The solar log *gf*'s of Peterson & Carney (1989) were derived by assuming a lower solar abundance by 0.15 dex, so we ought to reduce the *gf*'s by this amount to compensate for the higher solar abundance we work with. However, we found that systematic differences showed up in the program-star analysis, suggesting a reduction in the original values by 0.25 dex was required to match lines on the Froese Fisher scale, one of which is the predominant 3829 Å line. The final abundances were computed using this offset. The one remaining line was λ3838, for which Luck & Bond (1981) gave a log *gf* of +0.82, but this yielded very different abundances than neighboring lines of the same excitation potential. We instead adopted log $gf = -0.10$ to eliminate systematic differences between the 2.7 eV lines.

Aluminum.—The solar Al abundance, 6.47, is based on Lambert & Luck's (1978) analysis of red lines using theoretical *gf*-values. Our analysis uses the 3961 Å resonance line.

Calcium.—The adopted solar Ca abundance, 6.34, is in agreement with the meteoritic value and that based on ionized lines analyzed by Lambert & Luck (1978). However, Lambert & Luck's analysis of neutral lines yielded 6.54. Smith & O'Neill (1975) had suggested a different oscillator strength scale with the neutral *gf*'s up (and hence solar Ca I abundance down) by 0.11 dex. Since we rely on Ca I lines and the Smith & O'Neill scale, it is possible that a solar abundance of 6.43 would be more appropriate than 6.34 as the reference abundance for the lines studied in our stars. This 0.1 dex uncertainty should be borne in mind if attempting to interpret the absolute level of the Population II [Ca/Fe] value.

Titanium.—Grevesse, Blackwell, & Petford (1989) revised the Oxford neutral Ti oscillator strengths upward (and solar abundance downward) by 0.056 dex, giving a solar abundance on the new scale of 4.99. Since these changes balance one another, studies using the old Oxford scale and old solar scale will have arrived at the same stated value of [Ti/Fe] as they would have with the new scales.

3.4. *Abundance Computations*

Abundances were computed by using Kurucz's LTE WIDTH6 code. The derived gravity, iron abundance (based on neutral lines), and microturbulence for each star are recorded in Table 1. Subsequent columns indicate how many Fe I lines were used and the standard deviation of the abundances. Of the 19 stars for which we present new observations here, 10 have [Fe/H] < −3.0, and two of these have [Fe/H] < −3.5. In addition, we recomputed abundances for six stars by using all available equivalent width measurements from the literature. That analysis was conducted identically (and blind) to the one using only our own data.

Abundances for other elements are listed in Table 2. The first line in the table gives the adopted solar abundances. Two records are listed for each star: the first shows [Fe/H] and [X/Fe] (where X = other atomic species), and the second indicates how many lines were used. If only a single line contributed, its wavelength is given. As with Table 1, the first block presents data based on our equivalent width measurements, and the second presents results from reanalysis of six extremely metal-deficient stars using the extended line list.

Microturbulent velocities were obtained from Fe I lines with $W < 100$ mÅ by demanding no dependence of derived abundance on equivalent width. For the latter, we use the equivalent width expected for the inferred abundance rather than that directly measured, to avoid the correlated errors in individual line equivalent widths and abundances (Magain 1984).

As noted in § 3.1, the Fe I–to–Fe II ionization balance was used to constrain the surface gravities where possible.

3.4.1. *Error Estimates*

Errors in the equivalent widths, discussed extensively in Paper I, not only affect individual line abundances but also how well the microturbulence and surface gravity can be constrained. Spectra with S/N < 35 pixel^{-1} at 4300 Å generally suffer from poorly constrained model atmospheric parameters. Other errors affecting the abundances include inaccurate *gf*-values, errors in the adopted $T_{\rm eff}$, and unrecognized line blends, although we have guarded against the latter as much as possible. Systematic errors also arise in the spectral reduction, continuum placement being a common problem with low-S/N data and in crowded spectra; these are less problematic in weak-lined stars.

For each star, we compute the error in the mean iron abundance as follows, combining each term in quadrature: The dispersion of abundances for individual Fe I lines, $\sigma_{\rm Fe\ I}$, is listed in Table 1; we reduce this by a factor of $n^{1/2}$ (for n Fe I lines) to find the *minimum* random error for each star, giving rise to values from 0.01 to 0.05 dex. To that we add 0.1 dex per 100 K random error in $T_{\rm eff}$. Further contributions to the error come from the uncertainty in microturbulence, for which we add 0.06 dex, assuming uncertainty of order 0.2 km s^{-1}, and from errors in the gravity, for which we add another 0.04 dex. In Paper I, we identified systematic errors in some equivalent width comparisons that reach ∼10%. Since these systematics vary from star to star even within a given study, they mimic random errors among an ensemble of stars, so we add another 0.04 dex to the error estimate to allow for 10% errors in weak lines. The resulting errors for the iron abundances (from neutral lines) are typically 0.1 dex, and are listed in Table 1 (column $\epsilon_{\rm Fe\ I}$). These estimates do not include allowance for systematic revisions of the effective temperature scales.

We handle the relative abundances as follows: Errors in the atmospheric parameters affect the abundance calculation, errors in the line measurements affect the input data, and uncertainties in the derived iron abundance affect the reference value. We treat each of these separately. In this discussion, we ignore global systematics such as in the solar abundances since these influence all stars in our sample equally. We compute the effects of the uncertainties for three stars: HD 122563 (a giant), HD 140283 (a subgiant with the highest S/N in our sample), and CS 29527−015 (a dwarf with the lowest S/N of any of our data).

[4] We note that the 4571 Å line is a resonance line whereas the Froese Fisher lines come from 4.35 eV levels. It is possible that the difference between the abundances derived for the Thévenin line and the Froese Fisher lines (4703 Å in particular) are due not to the *gf*-values but to systematic errors in the adopted stellar effective temperatures or temperature structures of the model atmospheres. In anchoring our Mg analysis to the Froese Fisher values, we are anchoring to high-excitation lines.

TABLE 2

ABUNDANCES FOR PROGRAM STARS

Star	Fe I	Fe II	Mg I	Al I	Si I	Ca I	Sc II	Ti I	Ti II	Cr I	Cr II	Mn I	Co I	Ni I	Sr II	Y II	Zr II	Ba II	Eu II
The Sun[a]	−4.50	−4.50	−4.42	−5.53	−4.45	−5.64	−8.90	−7.01	−7.01	−6.33	−6.33	−6.61	−7.08	−5.75	−9.10	−9.76	−9.34	−9.87	−11.49
Based on Equivalent Widths Measured by Norris et al. (1996a, Table 1)																			
CD −38°245.....	−3.96	−0.07	+0.51	−0.80	+0.19	+0.27	+0.02	...	+0.26	−0.67	...	...	+0.41	−0.05	−0.62	<−0.27	...	<−0.97	...
	69	4233	3	3961	3905	2	3	...	23	3	...	...	3	4	2	3774	...	4554	...
CS 22897−008...	−3.19	−0.02	+0.41	−0.61	+0.67	+0.07	+0.13	−0.13	+0.38	−0.49	...	−0.55	+0.58	+0.62	+0.33	+0.33	...	−1.31	...
	96	4	5	3961	3905	4	4	3	27	3	...	3	5	5	2	6	...	4554	...
CS 22952−015...	−3.31	−0.01	+0.38	−0.51	+0.45	+0.07	−0.07	+0.05	+0.09	−0.70	...	−0.74	+0.28	+0.04	−0.88	−0.75	...	−1.46	...
	104	6	3	3961	3905	4	5	3989	27	3	...	3	4	4	2	3774	...	4554	...
CS 22172−002...	−3.57	+0.01	+0.49	−1.11	+0.23	+0.03	−0.08	+0.28	+0.24	−0.65	...	−1.06	+0.54	+0.09	−1.36	<−0.55	...	−1.17	...
	88	2	3	3961	3905	3	4	3	25	3	...	3	5	5	2	3774	...	4554	...
HD 122563	−2.68	+0.04	+0.32	−0.24	+0.58	+0.14	+0.25	+0.12	+0.34	−0.39	+0.07	−0.37	+0.33	+0.21	−0.21	−0.16	−0.10	−0.84	<−0.66
	165	15	7	3961	3905	9	7	10	32	7	2	5	5	9	2	5	4211	4554	4129
CS 22186−005...	−2.77	+0.02	+0.48	−1.18	−0.27	+0.19	−0.11	...	+0.10	−0.24	...	...	<+0.42	−0.28	−1.23	<−0.39	...	...	...
	58	9	3829	3961	3905	2	3	...	17	2	...	...	3873	2	2	3774	...	...	...
BS 16547−049...	−3.01	+0.02	+0.49	−0.76	+0.38	+0.47	+0.28:	+0.64	+0.33	−0.26	...	−0.55	...	−0.10	−0.04	<−0.51	...	−0.63	<+1.51
	67	2	3	3961	3905	5	2	3998	21	3	...	4033	...	2	2	3774	...	4554	4129
CS 22943−137...	−3.22	+0.48	+0.65	−0.64	+0.27	+0.01	−0.06	...	+0.18	−0.39	...	−0.46	+0.76	+0.50	<−1.43	<−0.24	...	<−0.43	...
	58	4583	4	3961	3905	4226	4246	...	11	3	...	3	3	4	4077	3774	...	4554	
CS 30308−062...	−2.92	−0.02	+0.43	−1.15	+0.16	+0.34	−0.16	...	+0.26	−0.45	...	−0.57	+0.32	+0.11	−0.68	<−0.04	...	<−0.47	<+1.72
	55	2	3829	3961	3905	3	4246	...	13	3	...	3	3894	3858	2	3788	...	4554	4129
HD 140283	−2.54	−0.01	+0.24	−1.02	+0.42	+0.43	+0.10	+0.21	+0.27	−0.07	+0.16	−0.48	+0.32	+0.07	−0.44	+0.18:	<+0.25	−0.91	<+0.57
	153	13	5	3961	3905	10	6	9	35	6	2	5	6	7	2	2	4211	4554	4129
BS 16472−070...	−2.71	−0.01	+0.26	−0.79	+0.04	+0.38	+0.15	...	+0.50	−0.18	...	−0.53	+0.76	−0.09	−0.13	<+0.84	...	−0.19	<+1.78
	65	2	2	3961	3905	6	2	...	17	3	...	2	2	4	2	3950	...	4554	4129
BS 16968−061...	−3.08	...	+0.48	−0.74	+0.19	+0.27	+0.53	...	+0.66	−0.32	...	−0.70	+0.63	+0.05	−0.50	<+0.67	...	<−0.18	<+2.01
	64	...	3	3961	3905	3	2	...	15	3	...	4030	3873	3	2	3788	...	4554	4129
CS 22166−030...	−3.36	...	+0.76	−0.80	−0.02	+0.24	+0.10	...	+0.76	−0.35	...	<−0.66	<+0.61	+0.19	−0.27	<+0.86	...	<+0.00	<+2.20
	47	...	2	3961	3905	4226	4246	...	9	2	...	4030	3873	2	2	3788	...	4554	4129
CS 22953−037...	−2.94	...	+0.40	−0.96	−0.19	+0.29	+0.06	...	+0.32	−0.48	...	<−0.71	<+0.37	+0.13	<−1.23	<+0.38	...	<−0.20	...
	56	...	3	3961	3905	2	4246	...	12	2	...	4030	3894	2	4077	3774	...	4554	...
CS 29491−084...	−2.74	−0.10	+0.14	−1.01	−0.03	+0.23	+0.30	...	+0.51	−0.30	...	−0.21	+0.53	−0.14	−0.16	<+0.47	...	<−0.37	<+1.81
	57	4233	2	3961	3905	5	2	...	18	3	...	4034	2	3858	2	3788	...	4554	4129
CS 29499−060...	−2.63	+0.01	+0.18	−1.03	−0.02	+0.25	+0.14	...	+0.55	+0.04	...	−0.41	<+0.40	+0.23	−0.43	<+0.11	...	<−0.46	...
	65	3	3	3961	3905	6	2	...	21	3	...	3	4121	4	2	3774	...	4554	...
CS 29527−015...	−3.43	...	<+0.78	...	...	+0.55	+0.54	...	<+0.53	<−0.06	...	<−0.08	<+1.30	<+1.60	+0.81:	<+1.42	...	<+0.37	<+2.62
	14	...	4703	...	...	4226	4246	...	4443	4254	...	4030	4121	4231	2	4374	...	4554	4129
G108−33	−2.69	...	+0.62	−0.65	+0.50	+0.03	<+0.11	...	+0.25	−0.49	...	...	...	+0.28	−0.16	<+0.37	...	<−0.47	<+1.71
	47	...	3829	3961	3905	2	4314	...	9	2	...	...	...	3858	2	3788	...	4554	4129
Based on Compilation by Norris et al. (1996a, Table 2)																			
CS 22876−032...	−3.85	<+0.06	+0.69	−0.26	−0.03	+0.10	<−0.43	...	<+0.50	<+0.04	...	+0.29	<+1.11	+0.21	<−0.48	...	...	<+0.54	...
	35	5169	3	3961	3905	4226	4246	...	3900	4254	...	4030	3845	3858	4077	...	...	4554	...
CS 22885−096...	−3.60	−0.02	+0.57	−0.81	+0.54	+0.46	+0.17	+0.51	+0.16	−0.63	...	−0.82	+0.28	−0.06	−1.54	...	...	<−0.74	+1.00
	96	7	7	3961	3905	5	4	4534	21	4	...	2	3	2	2	...	...	4554	3819
CS 22897−008...	−3.34	+0.04	+0.26	−0.66	+0.75	+0.24	+0.13	+0.14	+0.38	−0.42	...	−0.40	+0.66	+0.59	+0.40	+0.42	...	−1.17	...
	144	8	8	3961	3905	7	4	5	33	4	...	4	6	5	2	6	...	2	...
CS 22952−015...	−3.26	+0.01	+0.24	−0.49	+0.37	+0.16	−0.13	+0.01	+0.01	−0.56	...	−0.72	+0.23	−0.03	−0.87	−0.78	...	−1.45	+0.39
	143	14	5	3961	3905	8	5	3	29	5	...	3	6	4	2	3774	...	4554	4129
CS 22968−014...	−3.43	+0.02	+0.64	−0.90	+0.01	+0.22	+0.11	+0.33	+0.27	−0.57	...	−0.57	+0.83	+0.52	−1.81	...	...	<−1.49	...
	130	4	6	3961	3905	5	5	4	27	5	...	3	2	3	2	...	...	4554	...
CD −38°245.....	−3.92	+0.01	+0.48	−0.84	+0.35	+0.40	+0.26	+0.35	+0.39	−0.50	...	−1.18	+0.30	−0.15	−0.53	<−0.31	...	<−0.72	...
	109	5	3	3961	3905	4	6	3998	25	5	...	3	4	4	2	3774	...	4554	...

NOTE.—The table provides two records for each program star: the first lists the [Fe/H] value based on neutral lines followed by abundances relative to iron [X/Fe] for the remaining species (including Fe II). The second indicates how many lines were used in the analysis of each species, or in cases in which only one line was used, the wavelength of that line is given.

[a] Solar abundance log (N(X)/N(H)) adopted in the analysis.

Errors in the atmospheric parameters.—These cause the wrong stellar atmospheric model to be used. Fortunately, many elements respond to these errors in a similar way as iron, so only small differences arise in the [X/Fe] ratios. When an abundance is computed, a wrong $T_{\rm eff}$ will result in different gravities and microturbulence being inferred. We ignore this complexity and compute the changes in the abundance ratios separately for $\Delta T_{\rm eff} = +100$ K, for $\Delta \log g = +0.3$ dex, and for $\Delta\xi = +0.5$ km s^{-1} and then combine them in quadrature as if they were independent. These are treated as a 2 σ errors since the 100 K $T_{\rm eff}$ offset used here exceeds the ϵ_T-values given in Table 1, and the gravities and microturbulent velocities were usually determined to better than 0.3 dex and 0.5 km s^{-1}, respectively.

Random errors in the line measurements.—In Paper I, we derived for each star two estimates of the equivalent width uncertainty, one based on the recorded S/N and the other based on dual measurements of lines that fell in two echelle spectral orders. We adopt the larger of these estimates for each star, increase all measurements by this amount, and recompute the abundances. This clearly overestimates the error since not all lines will change systematically in this fashion, but it allows us to see the effects on saturated lines. The abundance change found is reduced by a factor of $N^{1/2}$ and then compared to the internal scatter (standard error) of that element's measured abundances. The larger of these values is adopted, which is usually the latter since it includes error contributions from the *gf*-values and from non-Gaussian measurement errors such as varying accuracy in the continuum fit, undetected line blends, and flat-fielding errors.

Errors in the reference iron abundance.—The error term added for [Fe/H] is $\sigma_{\rm Fe\,I}/n_{\rm Fe\,I}^{1/2}$ from Table 1; generally it is negligible.

The uncertainties are combined in quadrature to produce total [X/Fe] error estimates for the three stars, which are presented in Table 3. Temperature changes of 100 K have little effect on most relative abundances. For HD 122563 and HD 140283, final errors in most relative abundances are of order 0.05–0.10 dex. Occasionally, however, a larger error will raise its head where two lines yield poor agreement. Such cases have already been flagged in Table 2. CS 29527−015 is a worst-case calculation, this star having considerably lower S/N than is typical for our sample and having most abundances based on only a single line, so no benefit could be obtained from averaging. Consequently, its errors are dominated by the observational uncertainties. The errors in other dwarfs may be assessed by adopting the atmospheric errors computed for this star and reducing its observational errors according to the better S/N and greater numbers of lines sampled in the other stars. A more typical case with S/N = 40 and abundances derived from two to four lines would have errors in [X/Fe] of 0.13–0.10 dex.

3.4.2. *Hyperfine-Structure Effects*

For some spectral lines with significant hyperfine structure, a single-line approximation is inadequate. Hyperfine splitting distributes the line opacity across a greater wavelength range, so a line can grow to greater overall strength before saturating. The abundance derived if one ignores hyperfine structure therefore overestimates the true abundance. Artificially elevating the microturbulence is one way in which the effects of hyperfine structure may be approximated (see, e.g., Peterson 1981 [appendix]).

Hyperfine structure affects elements of odd atomic number and those with significant isotope splittings, but computations by Peterson (1981), Gratton & Sneden (1991), and McWilliam et al. (1995a) have shown that, for many of the lines in our study, hyperfine structure can be ignored at the line strengths we encounter. Specifically, we ignore hyperfine effects in the Al 3961 Å resonance line and in Sc, Sr, and Eu since the strongest Eu line analyzed in this paper has an equivalent width of only 16 mÅ.

For Mn and Co, however, ignoring hyperfine structure could lead to abundance errors of up to 0.6 dex. For these elements we proceed as follows: The six Mn lines in our analyses are included in Booth, Shallis, & Wells' (1983) tabulation of wavelength splittings and relative intensities measured with the Oxford absorption furnace. We computed synthetic line profiles for two cases: in the first the detailed line splitting was included, and in the second only a single line with the same overall *gf*-value was used; the difference in equivalent width was noted for a range of abundances. This procedure was performed for a turnoff-star model $T_{\rm eff}$/log g/[Fe/H]/ξ = 6200/4.0/−2.0/1.0, for a subgiant model 5800/3.5/−3.0/1.5, and for a giant model 4800/2.0/−3.0/2.5. Only the three ground-state lines are strong enough to be affected. The results are presented in Figures 1*a*–1*c*, in which we show for each wavelength the abundance error that results from the neglect of hyperfine splitting. This value must be added to the abundance derived from a single-line computation.

The process was repeated for cobalt, with line splittings computed from the interaction constants of Guthöhrlein & Keller (1990) and relative intensities taken from White & Eliason (1933). The results are shown in Figures 1*d*–1*g* for four of our wavelengths. Computations were also carried out for the 3842 Å line, but the effects were found to be negligible. For Co $\lambda\lambda$3873.96, 3995, hyperfine structure could not be computed. These lines are included in the abundance computations for six stars, but it is expected that their inclusion will contribute little error. The median correction for other stars was only −0.04 dex with a maximum of −0.18 dex. Since the unevaluated lines contribute only one-fourth or one-fifth of the final abundance (in the average of four or five lines), even sizable hyperfine-structure corrections for these two lines would have minor influence on the final results.

Ryan et al. (1991) neglected hyperfine structure in their study on the grounds that only weak-lined stars were being studied. However, as Figure 1 illustrates, even quite weak lines of Mn and Co can exhibit large errors. For this reason, the Mn and Co abundances of Ryan et al. have been revised by using the present computations. The median correction for Mn is only −0.03 dex, but four stronger lined stars had their abundances reduced by 0.3–0.4 dex. For cobalt the median correction was −0.07 dex, to a maximum of −0.49 dex. The revised abundances are used in the comparisons that appear later in this paper.

3.4.3. *Iron Abundances*

A few stars require special mention:

CS 22171−016 is a double-lined spectroscopic binary, the systemic velocity and velocity separation of which are recorded in Table 1 of Paper I. The secondary has Fe I lines approximately half the strength of those in the primary, so it probably contributes one-third of the continuum, in

1996ApJ...471..254R

TABLE 3

ERROR ESTIMATES FOR THREE PROGRAM STARS

A.

PARAMETER	HD 122563	HD 140283	CS 29527−015
S/N	110	232	28
$\sigma(W)$[a] (mÅ)	3	2	9
Standard error (Fe I)	0.016	0.011	0.043
ϵ_T	30	50	50

B.

	HD 122563						HD 140283						CS 29527−015					
	Δ[X/Fe]			1 σ			Δ[X/Fe]			1 σ			Δ[X/Fe]			1 σ		
RATIO	$T_{\rm eff}$	log g	ξ	Atm	Obs	Total	$T_{\rm eff}$	log g	ξ	Atm	Obs	Total	$T_{\rm eff}$	log g	ξ	Atm	Obs	Total
[Mg/Fe]	+0.00	−0.02	+0.04	0.02	0.04	0.04	−0.02	+0.00	+0.07	0.04	0.08	0.09	−0.04	+0.02	+0.10	0.05	0.12	0.13
[Al/Fe]	−0.01	−0.13	−0.12	0.09	0.05	0.10	+0.00	+0.01	−0.01	0.01	0.05	0.05	...	...	...	...	...	...
[Si/Fe]	+0.03	−0.10	+0.00	0.05	0.03	0.06	+0.05	−0.09	−0.03	0.05	0.02	0.05	...	...	...	...	...	...
[Ca/Fe]	−0.01	+0.05	+0.07	0.04	0.05	0.06	−0.02	+0.00	+0.05	0.03	0.03	0.04	+0.01	−0.08	−0.07	0.05	0.17	0.18
[Sc/Fe]	−0.05	+0.13	−0.07	0.08	0.07	0.11	−0.04	+0.13	+0.04	0.07	0.03	0.08	−0.04	+0.12	+0.07	0.07	0.19	0.20
[Ti I/Fe]	+0.02	+0.03	+0.05	0.03	0.04	0.05	+0.01	+0.03	+0.09	0.05	0.03	0.06	−0.01	+0.01	+0.08	0.04	0.22	0.22
[Ti II/Fe]	−0.06	+0.13	−0.03	0.07	0.03	0.08	−0.04	+0.12	+0.02	0.06	0.03	0.07	−0.05	+0.12	+0.08	0.08	0.23	0.24
[Cr I/Fe]	−0.01	+0.00	−0.04	0.02	0.07	0.07	+0.02	+0.02	+0.01	0.02	0.07	0.07	+0.01	+0.02	+0.08	0.04	0.23	0.23
[Cr II/Fe]	−0.10	+0.21	+0.11	0.13	0.14	0.19	−0.09	+0.14	+0.09	0.09	0.08	0.12	...	...	...	...	...	...
[Mn/Fe]	+0.01	−0.02	−0.07	0.04	0.03	0.05	+0.02	+0.02	+0.01	0.02	0.04	0.04	+0.01	+0.02	+0.08	0.04	0.23	0.23
[Fe I/H]	+0.08	−0.11	−0.12	0.09	0.02	0.11	+0.09	−0.03	−0.10	0.07	0.01	0.07	+0.09	−0.02	−0.10	0.07	0.04	0.08
[Fe II/Fe I]	−0.08	+0.19	+0.07	0.11	0.04	0.12	+0.01	+0.13	+0.07	0.08	0.03	0.09	...	...	...	...	...	...
[Co/Fe]	−0.02	−0.04	−0.12	0.06	0.03	0.07	+0.02	+0.03	+0.03	0.02	0.03	0.04	+0.01	+0.02	+0.08	0.04	0.24	0.24
[Ni/Fe]	−0.02	−0.02	−0.06	0.03	0.07	0.08	+0.00	+0.02	−0.02	0.01	0.04	0.04	−0.04	+0.03	+0.07	0.04	0.24	0.24
[Sr/Fe]	−0.03	+0.01	−0.18	0.09	0.04	0.10	+0.00	+0.07	−0.18	0.10	0.06	0.12	−0.01	+0.07	−0.07	0.05	0.35	0.35
[Y/Fe]	−0.05	+0.14	+0.02	0.08	0.06	0.10	−0.03	+0.14	+0.08	0.08	0.44	0.45	−0.04	+0.12	+0.07	0.07	0.24	0.25
[Ba/Fe]	−0.02	+0.13	−0.11	0.09	0.05	0.10	−0.02	+0.13	+0.07	0.07	0.06	0.09	−0.02	+0.11	+0.07	0.07	0.24	0.25
[Eu/Fe]	−0.02	+0.17	+0.12	0.10	0.22	0.24	−0.03	+0.13	+0.09	0.08	0.15	0.17	−0.03	+0.12	+0.07	0.07	0.26	0.27

NOTES.—The table gives the change in [X/Fe] (where Fe is from neutral lines) resulting from adjustments in the atmospheric parameters, except for Fe I itself, whose tabulation is for [Fe/H]. Three changes were made to the atmospheres, but only one at a time: $\Delta T_{\rm eff} = +100$ K, $\Delta \log g = +0.3$, $\Delta\xi = +0.5$ km s^{-1}. Three values of σ are tabulated: the first is the contribution from uncertain stellar atmospheric parameters, and the second is from the elemental measurements. The third is the quadratic sum of the atmospheric and observational errors, and may be interpreted as the standard error in the abundance ratio. The three atmospheric contributions tabulated under the heading Δ[X/Fe] are treated as 2 σ values.

[a] The adopted $\sigma(W)$ is the greater of the two estimates made in Paper I.

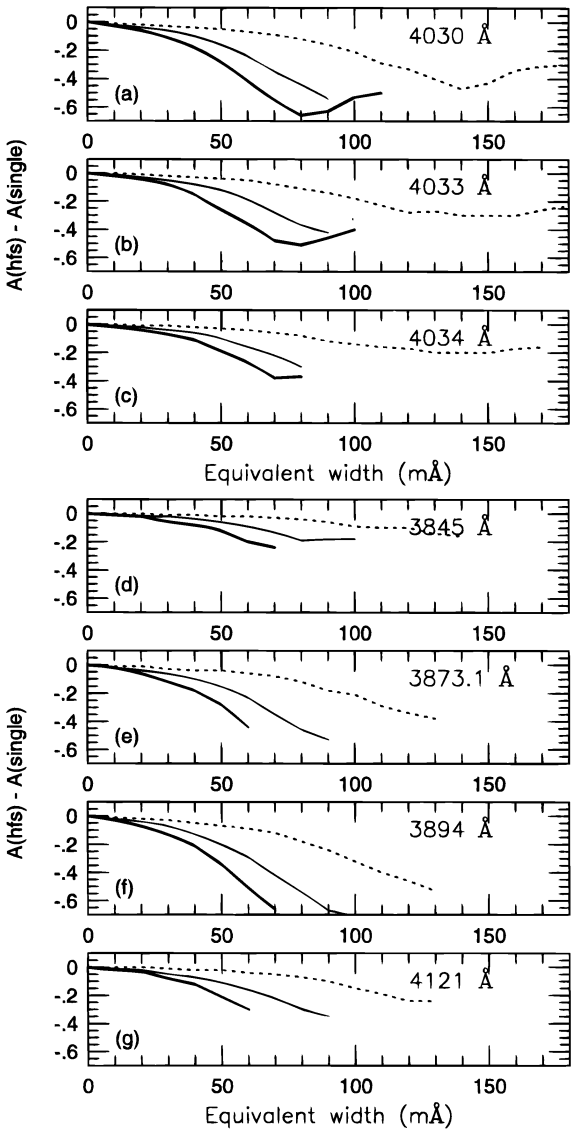

FIG. 1.—The error in abundance inferred for (*a–c*) three resonance lines of Mn and (*d–g*) four lines of Co through the neglect of hyperfine structure, as a function of observed equivalent width. Three models were considered, representative of turnoff stars (6200/4.0/−2.0/1.0) (*heavy curves*), subgiants (5800/3.5/−3.0/1.5) (*light curves*), and giants (4800/2.0/−3.0/2.5) (*dashed curves*).

which case the lines measured for the primary must be multiplied by 1.5. If the secondary is cooler, the factor should be less than 1.5. It is also possible that the primary is evolved and therefore cooler than the secondary. We compute iron abundances for two cases: (1) W(primary) = W(measured) and (2) W(primary) = 1.5W(measured). Systematic errors will be greater in this star than in others, and indeed the results were rather unsatisfactory. Case 1 demanded a very low microturbulence, which was fixed at 1.0 km s^{-1}, yet required a gravity typical of a horizontal-branch star to achieve ionization equilibrium. Case 2 yielded a more reasonable result but still with a gravity more typical of horizontal-branch stars. These "strange" results probably reflect systematic errors in our attempts to analyze a composite spectrum and in the use of an effective temperature based on composite colors. The errors for this star are consequently greater than for the remainder of our sample, and we exclude it from our discussion of abundances.

CS 22943−137 has a $B-V$ color similar to HD 140283, but the single Fe II line points toward a lower surface gravity, log g = 2.6. Rather than let the surface gravity be driven by a single spectral line, we have fixed the gravity at log g = 3.5.

The Fe I–to–Fe II ionization balance in CS 22186−005 verified its classification by Beers et al. (1992b) as a field horizontal-branch star. Furthermore, this star was the only one in our sample to have noticeably broadened spectral lines, corresponding to rotational broadening of $v \sin i = 9 \pm 1$ km s^{-1}.[5]

3.4.4. *Abundances of Other Elements*

Before discussing the astrophysical implications of these abundances, we mention a few additional points about the analysis.

Aluminum.—Arpigny & Magain (1983) warned that the 3944 Å line was blended with CH in some stars. In our spectra (which have a resolving power of 40000) of CS 22897−008, G108−33, HD 140283, and HD 122563, and possibly also in BS 16547−049 and CS 29499−060, this line is noticeably broader than neighboring lines of similar depth. We compared abundances for the two resonance lines in the remaining stars and obtained abundances 0.0–0.5 dex higher from the 3944 Å line. For this reason, we do not utilize abundances from the 3944 Å line.

The 3961 Å line is close to the Hε + Ca II H line. Ryan et al. (1991) argued that, in dwarfs, the greatest error introduced by depression of the local continuum was less than 0.06 dex. The effect will be even smaller in the cool giants, and we exclude making any correction for it.

Utilization of the Al I resonance lines has been questioned by François (1986), who quoted differences between results for these and for higher excitation red lines, the resonance lines yielding lower abundances. Gehren, Reile, & Steenbock (1991) investigated NLTE effects in Al, noting that neutral aluminum has the strongest ionization edge in the entire solar spectrum and that photoionization from the ground state should be extremely important. They concluded that the effects could be particularly great in metal-poor dwarfs. D. P. Baumueller & T. Gehren (1996, private communication) have since calculated NLTE corrections for the Al resonance line in metal-poor dwarfs, which show that LTE computations underestimate the abundances by 0.4–0.6 dex at [Fe/H] < −1.0. Furthermore, they noted that, quite apart from differences between LTE and NLTE analyses, the solar Al resonance lines yield abundances 0.2 dex lower than those from red and near-infrared lines, and it is red, high-excitation lines on which the reference (solar) abundance is based. We note for completeness that the meteoritic and solar photospheric abundances are in excellent agreement (Anders & Grevesse 1989). In very metal-poor stars, only the resonance lines are strong enough to measure. These issues will be important later when we discuss the zero point of the metal-poor star Al abundances.

Calcium.—Magain (1988) and Ryan et al. (1991) found that the Ca I resonance line at 4226 Å yielded abundances

[5] To obtain this estimate, we rotationally broadened the spectra of CS 22897−008 and CS 22952−015, which were observed during the same observing session as CS 22186−005, following Unsöld (1955, p. 508). These two comparison stars are sharp-lined giants, somewhat cooler than CS 22186−005 but of similar line strength. Within the assumptions, the value of $v \sin i$ is estimated to be accurate to 1 km s^{-1}.

PLATE 6

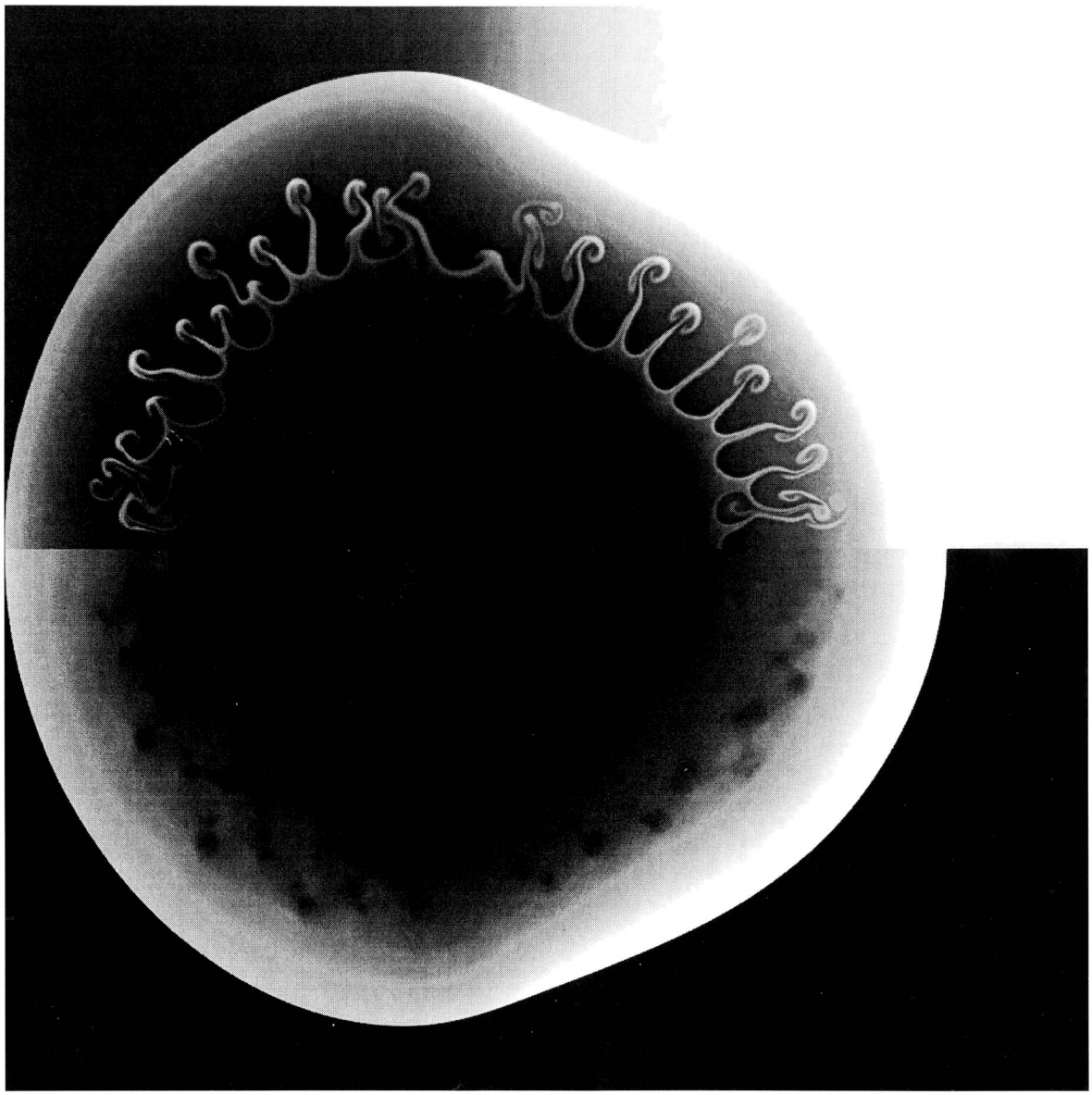

FIG. 6.—Gray-scale image of SNR3 at $\eta = 10$. The highest values are white, the lowest values are black. The top half is density that ranges from 90 to $1300 m_p$ cm^{-3}. The bottom half is pressure that ranges from 3.7×10^{-7} to 5.6×10^{-6} ergs cm^{-3}.

DOHM-PALMER & JONES (see 471, 283)

0.15 and 0.25 dex lower, respectively, than the 1.9 eV Ca I lines in their halo dwarfs. Our analysis utilizes a similar set of lines and models but covers a wider range of evolutionary types. For turnoff and subgiant stars, the mean abundance from the 4226 Å line was 0.18 dex lower than the mean of the others, with high consistency ($\sigma = 0.02$ dex). Consequently, we increased the abundance derived for the 4226 Å line in these stars by 0.18 dex, to make it consistent with results for the 1.9 eV lines. In particular this affects three stars for which only the 4226 Å line was measured. For the HB star and the giants, the dispersion was greater at 0.2 dex, but the mean difference was the same, so the same offset was applied.

4. COMPARISON WITH PREVIOUS OBSERVATIONS

In this section, we compare our abundances with those of previous investigators for stars in common. Those with [Fe/H] < -3 are compared in Table 4. Our adopted effective temperatures are generally higher by 0–250 K, reflecting the color–effective temperature scales adopted in § 3.1. It is not clear which scale is to be preferred. We note in this context that Norris et al. (1993) used excitation-based effective temperatures and that these were cooler by 0–200 K than the photometrically based effective temperatures they also derived. The subdwarf temperatures derived by Fuhrmann, Axer, & Gehren (1994) by fitting Balmer lines, on the other hand, are generally 100–200 K hotter than have typically been derived photometrically. These comparisons illustrate that systematic differences of this order are to be found between various studies and will propagate to the final abundances. Fortunately, most abundance ratios are considerably less sensitive to temperature errors than the absolute abundances themselves.

When an absolute analysis has been undertaken *and* described in detail, it is possible to compensate for different choices of the reference solar abundance. This is especially important for the solar iron abundance, which has ranged over 0.2 dex in recent studies. Before comparing our measurements with others from the literature, we have rescaled those from absolute analyses to the solar reference values in Table 2. Studies utilizing solar *gf*-values have been left unaltered.

TABLE 4

ANALYSES OF STARS IN COMBINED LINE LIST

Star/$T_{\rm eff}$	log g	[Fe/H][a]	ξ (km s^{-1})	Reference
CD −38°245:				
4800	2.0	−4.5	3.5	1
4700	1.4	−3.77	2.1	2
(GS88).....	(GS88)	−4.30	2.0	3[b]
4750	1.9	−3.91	2.5	4
(GS88).....	(GS88)	−4.13	2.0	5[b]
4730	1.8	−3.99	2.0	6
4850	1.5	−3.96	2.4	7
4850	2.0	−3.92	2.1	Compilation[c]
CS 22876−032:				
5900	4.0	−4.13	2.5	3
6000	4.0	−3.96	2.0	8
6100	4.0	−3.85	1.5	Compilation
CS 22885−096:				
4900	1.0	−4.05	2.0	9
4800	2.0	−4.07	2.5	8
4920	2.1	−3.77	2.2	6
5050	2.0	−3.60	1.8	Compilation
CS 22897−008:				
4790	1.5	−3.33	2.2	6
4850	1.8	−3.19	1.7	7
4850	1.8	−3.34	2.0	Compilation
CS 22952−015				
4720	0.9	−3.36	2.6	6
4850	1.6	−3.31	2.5	7
4850	1.4	−3.26	2.5	Compilation
CS 22968−014				
4800	2.0	−3.60	2.5	8
4950	2.0	−3.45	1.9	5
4840	1.8	−3.39	1.9	6
4950	1.8	−3.43	2.3	Compilation

[a] Adjusted to log $(N(\mathrm{Fe})/N(\mathrm{H}))_{\odot} = -4.50$.

[b] These adopt the temperature and gravity given by Gratton & Sneden 1988.

[c] Compilation entries are our analyses using all available line measurements, as discussed in the text.

REFERENCES.—(1) Bessell & Norris 1984; (2) Gratton & Sneden 1988; (3) Molaro & Castelli 1990; (4) Peterson et al. 1990; (5) Primas et al. 1994; (6) McWilliam et al. 1995a; (7) this work, using our own line measurements; (8) Norris et al. 1993; (9) Molaro & Bonifacio 1990.

4.1. *The "Control" Stars HD 122563 and HD 140283*

Our analysis of HD 122563 yielded [Fe/H] $= -2.68$, compared with the abundances derived by Gratton & Sneden (1994), viz., Fe I $= -2.81$, Fe II $= -2.66$. The agreement is very good.

Many observations of the subgiant HD 140283 were summarized by Ryan et al. (1991, Table 7). It suffices to note that our abundance, [Fe/H] $= -2.54$, is completely in line with previous determinations.

4.2. *CD −38°245*

The first analysis by Bessell & Norris (1984) yielded a lower abundance ([Fe/H] $= -4.5$) than most more recent analyses, primarily because their data implied high microturbulence, 3.5 km s^{-1}. Subsequent studies (Gratton & Sneden 1988; Molaro & Castelli 1990; Peterson, Kurucz, & Carney 1990; Primas, Molaro, & Castelli 1994; McWilliam et al. 1995a) and the present investigation have found microturbulence values in the range 2.0–2.5 km s^{-1}, more like the values found in less metal-poor halo giants. With the exception of Molaro & Castelli (1990), these studies obtained higher iron abundances, around [Fe/H] $= -4.0$. Our abundances, [Fe/H] $= -3.96$ from our own equivalent widths and [Fe/H] $= -3.92$ from the combined line set, are in good agreement.

4.3. *Stars from Beers et al. (1985, 1992b)*

Our reanalysis of CS 22876−032 yields [Fe/H] $= -3.85$, well above the abundances obtained by Molaro & Castelli (1990: −4.29) and by Norris et al. (1993: −4.13). However, both those studies adopted higher solar abundances (by 0.13 and 0.17 dex, respectively); renormalization to our adopted solar value raises these measurements to −4.13 and −3.96, as shown in Table 4. We derive a significantly lower microturbulence than the other two works, possibly as a result of adopting Magain's (1984) scheme; we obtain 1.5 km s^{-1}, relative to their 2.5 and 2.0 km s^{-1}. The new microturbulent velocity is obtained from the combined line list and is more in keeping with values obtained for other, more metal-rich, halo turnoff stars, whose microturbulent velocities tend to range between 1.0 and 1.5 km s^{-1}. This accounts for much of the upward revision in metallicity, along with a contribution from the higher effective temperature used here. We note for completeness that this star is a double-lined spectroscopic binary (Nissen 1989). The

implications of this have been discussed already by Norris et al. (1993, § 4).

The abundance for CS 22885−096 is comparatively high (−3.60) compared with the other analyses. Our effective temperature exceeds the excitation temperature of Norris et al. by 250 K and the photometric temperature of McWilliam et al. by 130 K, and this accounts for part of the difference. (As a rule of thumb, the derived iron abundance decreases by 0.1 dex for every 100 K increase in effective temperature.) Also contributing to the difference is the microturbulence, which was poorly constrained in the analysis. The inferred value (1.8 km s^{-1}) seems marginally below expectations for a giant.

Our own subset of lines in CS 22897−008 drove us to a lower microturbulence and slightly higher abundance than McWilliam et al. Use of the combined line list resulted in a higher microturbulence and left us in excellent agreement with the McWilliam et al. result.

Our analysis of CS 22952−015, both using our own line list and the extended line list, is again in good agreement with the results of McWilliam et al.

For the remaining star reanalyzed, CS 22968−014, our results essentially match those of Primas et al. and McWilliam et al. but differ from that of Norris et al. by $\simeq 0.15$ dex, driven by the higher temperature and lower microturbulent velocities derived in the more recent analyses.

5. DISCUSSION

In this discussion, we present figures that include data from other published studies, adjusted onto common solar-abundance scales where possible. For the six stars that we reanalyzed using extended line lists, we show only the new abundances and not the individual results based on smaller line lists. Where other stars have been studied in more than one investigation, we link the individual observations with solid bars. Only upper limits exist for some abundances. Where these exceed most other stars anyway, they have been treated as uninteresting and excluded from the plots. The other sources whose data we show are Barbuy, Spite, & Spite (1985), Bessell & Norris (1984), Carney & Peterson (1981), Gilroy et al. (1988), Gratton (1989), Gratton & Sneden (1987, 1988, 1991, 1994), McWilliam et al. (1995a), Magain (1987, 1989), Molaro & Bonifacio (1990), Molaro & Castelli (1990), Norris et al. (1993), Peterson (1981), Peterson et al. (1990), Primas et al. (1994), Ryan et al. (1991), and Zhao & Magain (1990). Since the results of Magain (1989) and Zhao & Magain (1990) pertain to the same set of stars, we have averaged their results, except for Ti, for which we use the older analysis which they preferred, and for Sc, Y, and Ba, for which Zhao & Magain reanalyzed the old data.

Since we have deferred our discussion of the stars with strong CH bands to Paper IV, we have also excluded the C-rich objects of McWilliam et al. (1995a) from this paper. Specifically, we have excluded those stars with [C/Fe] > 0.75 (see McWilliam et al.'s Fig. 26), viz., CS 22892−052, CS 22898−027, and CS 22947−187, *except* that we have not excluded CS 22949−037, for which it appears that the iron group rather than carbon is anomalous.

In a small number of cases in which there is overlap between different studies, we have been able to check for consistency among line-strength measurements. We have rejected two cases, both involving strontium: Gratton & Sneden's (1988) measurement in HD 140283, which exceeds all of the others by a considerable margin, and the observation of a 3.7 mÅ line in −18°5550 by Gilroy et al. (1988).

In our discussion of the relative elemental abundances as a function of [Fe/H], we make use of robust statistical tools to aid in assessment of the trends, employing the techniques described by Cleveland & Kleiner (1975). Measurements in which only upper limits were derived were not considered in this analysis. First, average values of each abundance ratio were obtained for stars measured by several workers. Next, we obtained three vectors, the midmean (MM), the lower semi-midmean (LSMM), and the upper semi-midmean (USMM), as a function of [Fe/H] values. These vectors are defined as follows: MM—an average of all observations between and including the quartiles of the data over a given range in [Fe/H]; LSMM—the midmean of all observations below the median; USMM—the midmean of all observations above the median. If the data are scattered about the midmean according to a normal distribution, the semi-midmeans are estimates of the true quartiles. In Figures 2–5, we take a running window containing 10% of the data, corresponding to 10–15 data points at a time. These results were then smoothed with a locally weighted regression line ("*lowess*"; see Cleveland & Devlin 1988).

To quantify the scale[6] of the data for each elemental ratio, we first obtain the *lowess* line as a function of [Fe/H], and then the residual in the ordinate of each data point about the trend. In Table 5, we summarize robust estimates of scale for these residuals over three ranges in [Fe/H], using the biweight estimator S_{BI} discussed by Beers et al. (1990a). In this table we also include an estimate of the 95% range in the residuals, obtained as $R_{95} = 2(1.96S_{BI})$, since $1.96S_{BI}$ is the one-sided 2 σ interval of a normal distribution.

5.1. *Iron Abundances*

Ten of the stars for which we obtained new spectroscopic data have [Fe/H] < −3.00. The lowest abundance we derive for a previously unobserved star is [Fe/H] = −3.57, for CS 22172−002. This brings to six the number of stars with high-resolution studies yielding [Fe/H] < −3.50 (on our adopted solar scale). We list these stars in Table 6. Only one of the stars, CD −24°17504, came to our attention as a result of its high proper motion; the remainder were identified through objective-prism surveys. This is because kinematics provides no discrimination between extremely metal-poor stars and the bulk of halo stars, whereas objective-prism surveys have the ability to select the most extreme examples of metal deficiency.

5.2. *The α-Elements: Magnesium, Silicon, Calcium, and Titanium*

It may be useful to remind the reader that although elements lighter than calcium are *expelled* in supernovae (SNs), they are chiefly *produced* by hydrostatic burning *before* the explosion. In contrast, heavier elements in the iron group are produced by explosive burning and are sensitive to the details of the explosion mechanism and its inherent uncertainties (K. Nomoto 1992, private communication; Timmes, Woosley, & Weaver 1995).

We also note that in their comparison of Galactic chemical evolution predictions and observations, Timmes et al. frequently record that "the departure from classical α-element abundances at [Fe/H] $\simeq$ −2.5 dex is primarily due

[6] The scale matches the dispersion for a normal distribution.

TABLE 5

ROBUST SCATTER ESTIMATES FOR ELEMENTAL RATIOS IN METAL-POOR STARS

[Fe/H] Range	N	S_{BI}[a]	R_{95}[b]
[Mg/Fe]:			
> -1.5	47	0.21	0.82
-2.5 to -1.5.....	47	0.17	0.67
≤ -2.5	60	0.17	0.67
[Si/Fe]:			
> -1.5	44	0.11	0.43
-2.5 to -1.5.....	31	0.14	0.55
≤ -2.5	47	0.32	1.25
[Ca/Fe]:			
> -1.5	54	0.11	0.43
-2.5 to -1.5.....	50	0.15	0.59
≤ -2.5	60	0.16	0.63
[Ti/Fe]:			
> -1.5	55	0.12	0.47
-2.5 to -1.5.....	48	0.13	0.51
≤ -2.5	58	0.20	0.78
[Al/Fe]:			
> -1.5	43	0.26	1.02
-2.5 to -1.5.....	41	0.48	1.88
≤ -2.5	58	0.33	1.29
[Al/Mg]:			
> -1.5	43	0.19	0.74
-2.5 to -1.5.....	40	0.44	1.72
≤ -2.5	57	0.36	1.41
[Sc/Fe]:			
> -1.5	23	0.13	0.51
-2.5 to -1.5.....	46	0.20	0.78
≤ -2.5	58	0.20	0.78
[Cr/Fe]:			
> -1.5	29	0.10	0.39
-2.5 to -1.5.....	44	0.11	0.43
≤ -2.5	58	0.19	0.74
[Mn/Fe]:			
> -1.5	31	0.16	0.63
-2.5 to -1.5.....	27	0.17	0.67
≤ -2.5	49	0.23	0.90
[Co/Fe]:			
> -1.5	22	0.18	0.71
-2.5 to -1.5.....	26	0.38	1.49
≤ -2.5	44	0.25	0.98
[Ni/Fe]:			
> -1.5	57	0.10	0.39
-2.5 to -1.5.....	47	0.15	0.59
≤ -2.5	55	0.24	0.94
[Sr/Fe]:			
> -1.5	16	0.15	0.59
-2.5 to -1.5.....	42	0.35	1.37
≤ -2.5	55	0.62	2.43
[Y/Fe]:			
> -1.5	17	0.11	0.43
-2.5 to -1.5.....	40	0.17	0.67
≤ -2.5	31	0.41	1.61
[Ba/Fe]:			
> -1.5	17	0.09	0.35
-2.5 to -1.5.....	39	0.30	1.18
≤ -2.5	33	0.55	2.16

[a] Robust biweight estimator of the scatter in the elemental abundance ratio about the mean trend over the stated range in [Fe/H].

[b] Estimate of the range occupied by 95% of the residuals, as discussed in § 5.

TABLE 6

HALO STARS WITH [Fe/H] < -3.50

Star	[Fe/H][a]	Type	High-resolution Studies
CS 22949−037	−3.97	G	1
CD −38°245	−3.92[b]	G	1, 2, 3, 4, 5, 6, 7
CS 22876−032	−3.85[b]	TO	5, 8
CS 22885−096	−3.60[b]	G	1, 8, 9
CS 22172−002	−3.57	G	7
CD −24°17504.....	−3.55	TO	10

[a] Using $\log (N(\mathrm{Fe})/N(\mathrm{H}))_{\odot} = -4.50$.

[b] Reanalyzed in this paper using a combined line list; see text for discussion.

REFERENCES.—(1) McWilliam et al. 1995a; (2) Bessell & Norris 1984; (3) Gratton & Sneden 1988; (4) Peterson et al. 1990; (5) Molaro & Castelli 1990; (6) Primas et al. 1994; (7) this work; (8) Norris et al. 1993; (9) Molaro & Bonifacio 1990; (10) Ryan et al. 1991.

to uncertainties in the extremely low metallicity $M \gtrsim 30\ M_{\odot}$ massive star models," presumably referring to the difficulty experienced by Woosley & Weaver (1995) in getting such compact, massive stars to eject any heavy elements rather than having the envelope collapse back down on the stellar remnant. This is a good reminder that stars of the metallicity observed in our study, $-4 < [\mathrm{Fe/H}] < -2.5$, were likely enriched by such very massive stars, and the observed abundances can provide valuable constraints on what appears a difficult theoretical task, namely, the prediction of yields for low-metallicity stars with $M \gtrsim 30\ M_{\odot}$.

Magnesium, along with sodium and aluminum, is believed to be produced in hydrostatic burning of carbon and neon in 10–30 $M_{\odot}$ stars. The same stars are responsible for the production of silicon and calcium both before and during the eventual Type II SN explosion (e.g., Woosley & Weaver 1986). We show the observed Mg, Si and Ca abundances in Figure 2. Also shown are the data for titanium.

The ejecta of Type Ia SNs contain a significantly higher proportion of iron than Type II SN ejecta, but Type Ia progenitors evolve much more slowly. The late-time appearance of Type Ia SN products, once the Galactic gas had been enriched to $[\mathrm{Fe/H}] > -1.0$, results in lower [α-element/Fe] values at higher abundances (see, e.g., Wheeler et al. 1989). The Type Ia SN progenitor lifetimes are, consequently, too great to explain the iron observed in halo stars and that too must arise in massive stars via explosive nucleosynthesis.

We superpose two curves from Timmes et al. (1995) on the data shown in Figures 2*e*–2*h*. The lower dotted curve gives their baseline Galactic chemical evolution calculation; the upper gives their result when massive-star iron yields were reduced by a factor of 2, which Timmes et al. found to provide a better match to the Mg observations. (The sensitivity of iron yields to uncertain details of the explosion justified this change.) Also shown in Figures 2*e*–2*h* (*solid curves*) are the robust trend lines determined from the observations, as described above. The other α-elements shown do not argue strongly against the lower iron yield. One point in favor of it is that the iron yield is so high in the baseline calculation that no downturn in the α-element abundances is predicted at $[\mathrm{Fe/H}] > -1$, when Type Ia SNs begin to contribute in the models. However, the existence of such a downturn is well established in the observations.

Figure 2*a* suggests, even ignoring the two data with $[\mathrm{Mg/Fe}] > +1$, that the [Mg/Fe] overabundance increases

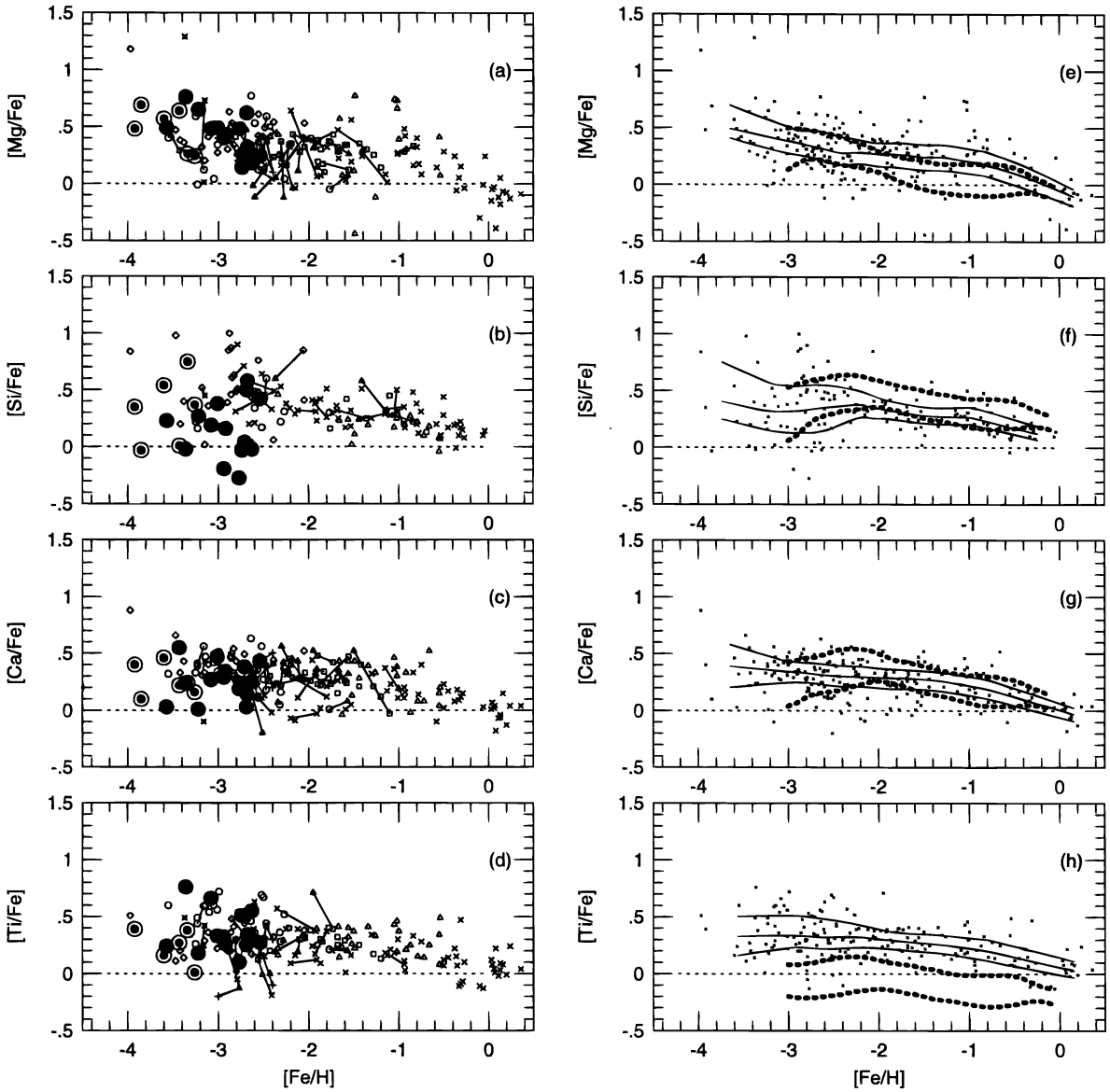

FIG. 2.—The α-element ratios. The left panels show the individual data from this paper (*solid circles*); our reanalysis of six stars (*circled dots*); Bessell & Norris (1984), Ryan et al. (1991), and Norris et al. (1993) (*open circles*); Magain (1987, 1989) and Zhao & Magain (1990) (*squares*); Gratton & Sneden (1987, 1988, 1991) and Gratton (1989) (*light crosses*); Carney & Peterson (1981), Peterson (1981), and Peterson et al. (1990) (*triangles*); Molaro & Castelli (1990), Molaro & Bonifacio (1990), and Primas et al. (1994) (*heavy crosses*); Gilroy et al. (1988) (*stars*); Barbuy et al. (1985) (*plus signs*); and McWilliam et al. (1995a) (*diamonds*). Multiple observations of a star are shown by solid links. The right panels show the same data overlaid by five curves. The central solid curve gives the robust trend computed from the data as described in § 5.2, flanked by the USMM and LSMM. The lower dotted curve gives the baseline Galactic chemical evolution model from Timmes et al. (1995). The upper dotted curve is their calculation with the massive-star Fe yield reduced by a factor of 2. (*a*) Mg. The two stars with [Mg/Fe] > +1.0 are CS 22949−037 (McWilliam et al. 1995a) and CS 22881−039 (Molaro & Bonifacio 1990). The former has widespread abundance anomalies; few data are available on the latter. (*b*) Si. Our abundances are based on only the 3905 Å line. (*c*) Ca. (*d*) Ti.

toward lower metallicity. The contrast with the flat relations for [Ca/Fe] and [Ti/Fe] makes this even more striking.[7] The existence of this trend is also clear from the robust fit in Figure 2*e*, which shows [Mg/Fe] increasing *without* the upper and LSMMs diverging; that is, the [Mg/Fe] trend is not merely meandering through noisy data. However, caution is required in case this behavior reflects systematic errors. For example, a small increase in [Ti/Fe] is observed in going from [Fe/H] ∼ −1.5 to [Fe/H] ∼ −2.5, but as discussed in Ryan et al. (1991), this accompanies a shift from the analysis of Ti I lines in the more metal-rich stars to reliance on Ti II lines in the more metal-poor ones, and the trend may be spurious. In more metal-poor stars, generally only a subset of the line list used in the more metal-rich stars can be utilized, so different lines contribute to the analysis. Even when the same lines are used, their weakening in metal-deficient stars means they form at different (greater) depths in the atmosphere, so errors in the atmospheric model (see § 3.2) could introduce metallicity-correlated effects. If the lines move through the saturated portion of the curve of growth, the sensitivity to abundance is rather low, and the sensitivity to errors in the outer layers of the model and to the microturbulence is rather high. Our analysis of Mg has relied largely upon the

[7] This behavior also contrasts with the results of McWilliam et al. (1995a), who found [Ca/Mg] and [Ti/Mg] to be slightly higher in the most metal-poor stars.

2.7 eV triplet at 3830 Å, supplemented in the compilation stars by measurements of the 5170 Å triplet. These lines have equivalent widths around 100–150 mÅ and clearly occupy the saturated region of the curve of growth. Until the result can be checked with observations of weaker lines or by using the same model atmospheric grid for all stars, the apparent trend should be viewed with caution.

Silicon abundances in extremely metal-poor stars are conventionally based on only a few lines. We exclude the 4102.9 Å line because in the dwarfs in our sample it lies in the wing of the broad Hδ line. A result of using only one line is that our abundances show considerable scatter, the dispersion being 0.28 dex, compared with 0.18 dex for [Mg/Fe]. The line also lies on the saturated portion of the curve of growth, so it is more sensitive to errors discussed previously. Our data yield a mean overabundance [Si/Fe] = 0.22 dex, identical to the result obtained for this line in slightly less extreme halo dwarfs by Ryan et al. (1991, rescaled solar). However, the result differs from McWilliam et al.'s finding of [Si/Fe] = 0.51, or 0.72 if strong 3905 Å lines were included. For the three stars for which we both measured Si, there is no evidence of a systematic difference in computations since, for two of these, we measured stronger 3905 Å equivalent widths than McWilliam et al. and derived greater Si abundances, and for the third, we measured the line as weaker and computed a lower abundance. The cause of this difference remains unresolved.

Observations of titanium in halo stars have long shown this element to have similar overabundances relative to iron as the α-elements do, whereas nucleosynthetic calculations suggest it is underproduced relative to iron (Timmes et al. 1995). The present data (Figs. 2*d*, 2*h*) show the overabundance continuing at least down to the limit of observation at [Fe/H] = −4, and it seems difficult to avoid concluding that Ti is overproduced in the supernovae of massive metal-poor stars. This is also consistent with the result that Type Ia SNs do not produce titanium as abundantly as iron (compare Figs. 4 and 5 of Timmes et al.); this will lead to the observed fall of [Ti/Fe] as [Fe/H] increases from −1 to solar, as Type Ia SNs contribute relatively more iron than titanium. It is clear that Ti yields from SN models depend sensitively on the details of the explosion (Nomoto 1992, private communication), with variations of ∼0.35 dex possible (Timmes et al. 1995). We trust that more advanced models may one day reproduce the observations.

5.3. *Aluminum*

Aluminum abundances are shown in Figure 3, both as [Al/Fe] and as [Al/Mg]. The new data extend the plateau of [Al/Fe] seen in Ryan et al. (1991) down to [Fe/H] = −4.0. The plateau appears particularly clear in the robust trend lines for [Al/Fe], though less so for [Al/Mg], which may reflect the increase in [Mg/Fe] at lower metallicity.

CS 22949−037, whose iron-group deficiency was highlighted by McWilliam et al. (1995a), and CS 22876−032 both have high [Al/Fe] abundances but "normal" values of [Al/Mg]. This is consistent with Al and Mg being produced under similar circumstances but by a different mechanism from Fe, as nucleosynthetic computations predict. Since Mg and Al reside much further out in an SN progenitor than the region where Fe is formed near the mass cut, it is reasonable that the expelled fractions of Mg and Al, on the one hand, and Fe on the other, should differ in different SNs, especially since models of massive, low-metallicity SNs experience greater difficulty in ejecting the inner layers (Woosley & Weaver 1995). One would expect to encounter cases in which less than the usual complement of Fe has been ejected, leading to higher [Al/Fe] and [Mg/Fe] values than normal. Furthermore, these events would lead to less contamination of the interstellar medium (ISM) by iron, so these divergent [Al/Fe] ratios would be more likely to be

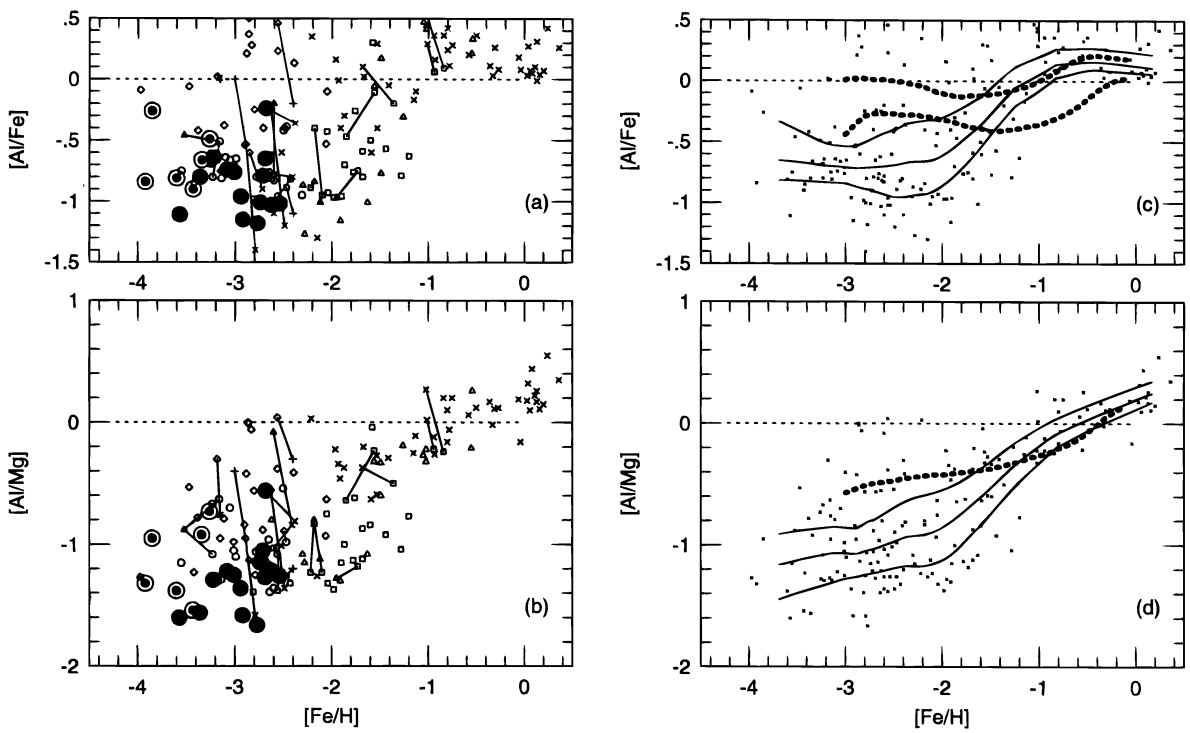

FIG. 3.—Al abundance ratios with (*a*, *c*) Fe and (*b*, *d*) Mg. Symbols and curves are as in Fig. 2, except that for [Al/Mg] only the baseline chemical evolution model from Timmes et al. is shown since this quantity is barely affected by the Fe yield.

observed at the lowest iron abundances, which correspond to times when massive, low-metallicity SNs existed. We note in this regard that CS 22949−037 and CS 22876−032 both have [Fe/H] $\simeq -4$.

A related observation for CS 22876−032 is that while its Mg and Al seem overabundant relative to Fe, the α-elements Si and Ca have essentially solar abundance ratios. It is as if the outermost layers processed by the progenitor have been pushed off into space but the deeper layers have not. Unfortunately, the scatter for Si is large, so it is unclear how significant its deficiency is. Efforts to obtain the Ti abundance of this star may be revealing.

Multiple studies of some stars exhibit poor repeatability, and often it is not possible to follow the analysis trail closely enough to discover the cause. McWilliam et al. (1995a) noted that the average [Al/Fe] value for their sample was higher than those of Gratton & Sneden (1988) and Magain (1987) by ∼0.5 dex. For the three stars we have in common with McWilliam et al., we derive very similar [Al/Fe] ratios, the differences being reasonably consistent with the different input equivalent widths; the mean difference is only 0.04 dex, and the largest difference is 0.16 dex. On a star-to-star level, our results agree with those of McWilliam et al. Is the spread in aluminum abundances significant? Since our analysis is based only on one transition, a spread as large as that found for the single silicon line would not be unreasonable (assuming [Si/Fe] to have negligible *intrinsic* spread consistent with the other α-elements). Indeed, for [Al/Fe], we obtain a dispersion of 0.26 dex about a mean of −0.80 dex, comparable with the 0.28 dex dispersion measured for [Si/Fe]. However, in Figure 3 we see stars at [Fe/H] ~ -3.0 that range up to more than 1.0 dex above the mean of our sample. It is these stars that dominate McWilliam et al.'s finding of a higher average [Al/Fe] for their sample than in previous studies, whereas our sample collapses to a fairly well defined plateau at [Al/Fe] $\simeq -0.8$. The reason for the higher average in the McWilliam et al. sample is unclear. We note for the record that no obvious dwarf versus giant differences are apparent in our study. (Our abundances in Table 2 show a statistically insignificant [1.2 σ] difference of 0.20 dex between the mean [Al/Fe] ratios for giants and turnoff stars, the latter being more Al-poor.) One effect of the higher abundances in the McWilliam et al. study is to drive the ensemble plateau higher in Figure 3*c*, to [Al/Fe] $\simeq -0.7$ dex.

Finally, we address the question of how well the stated plateau level is determined. Baumueller & Gehren (1996, private communication) have computed NLTE corrections for the Al I resonance lines in dwarfs arising from the strong ionization edge of this species. Their computations show that at [Fe/H] < -1, LTE treatments will underestimate the abundance by 0.4–0.6 dex. In this circumstance, the mean abundance quoted above, [Al/Fe] $\simeq -0.8$, should in reality be nearer −0.3 dex, still well below the [Mg/Fe] value and thus consistent with the presence of an odd-even effect for Al and Mg. We are not aware of how large a correction might be required for metal-poor giants, but we repeat that no significant dwarf-giant differences were obvious in our measurements. The (dwarf) NLTE plateau is above the −0.8 dex level "guessed" by Woosley (1982) for primary production of Al if metal-poor stars create their own neutron excess (necessary for Al nucleosynthesis) through C burning, but [Al/Fe] ~ -0.3 *is* what Timmes et al. computed for their baseline chemical evolution model. If their massive-star iron yields are halved, the ratio approaches solar. Timmes et al. computed [Al/Mg] ~ -0.5 dex in very metal-poor stars; this value is relatively insensitive to the iron yields. One other reason to question the absolute value of the plateau is that the resonance lines appear to lead to different abundances than higher excitation lines, as discussed earlier.

It is clear that much work remains to be done on aluminum. The abundance ranges require verification with high-S/N data and with stellar atmospheric parameters derived using systematic criteria. The line analysis needs to be performed using a consistent set of model atmospheres, and NLTE effects must be taken into account.

5.4. *The Iron-Group Elements*

Until recently, observations showed that the iron-group elements track iron depletion in metal-poor stars, with the exception of Mn, which showed an underabundance roughly mirroring the overabundance of the α-elements. Timmes et al. (1995) ascribed this behavior not to any effect of Type Ia SNs, but to metallicity dependence of the Mn yields of Type II SNs.

A recent highlight in studies of extremely metal-poor stars was the discovery of a change in abundance ratios of several iron-group elements around [Fe/H] $= -2.5$, which became apparent once the trends could be traced to [Fe/H] < -3.0 (McWilliam et al. 1995a). In Figure 4, we show our data on the elements from scandium ($Z = 21$) to nickel ($Z = 28$) with the exclusion of titanium and iron, which have already been discussed, and vanadium, for which there are few data. Figure 4 shows clearly that the new trends identified by McWilliam et al. for Cr, Mn, and Co are reproduced in our data: the two elements immediately below iron, Cr and Mn, drop to greater overdeficiencies at [Fe/H] < -2.5 whereas the next element above iron, Co, is seen to rise to higher abundances. (We remind the reader that the [Mn/Fe] and [Co/Fe] data of Ryan et al. 1991 have been corrected in Figure 4 for hyperfine-structure effects.) Sc appears to track the iron abundance as at higher halo metallicities.

The new data suggest that [Ni/Fe] may also increase toward lower metallicities, though not as steeply as [Co/Fe]. Both the individual data (Fig. 4*e*) and the robust trend lines (Fig. 4*j*) indicate this change, but it is important to be cautious in the interpretation and aware of possible systematics in the data. In particular, there are three stars in our sample around [Fe/H] $= -3.3$ that all appear overabundant in [Ni/Fe] by 0.5 dex (see Fig. 4*e*) whereas most other data are consistent with [Ni/Fe] $\simeq 0$. The results for these three stars are based on two to five Ni lines each and should not be seriously in error. Furthermore, from Table 3 we see that [Ni/Fe] is very insensitive to errors in the atmospheric parameters. The Ni I 4231 Å line, which McWilliam et al. warn can be blended with CH, was utilized only in the analyses of the more metal-rich stars HD 122563 and HD 140283, and in those cases there were numerous other lines confirming that this one was not abnormal. We note that the trend we tentatively identify for [Ni/Fe] is quite different from that the now overturned findings of Luck & Bond (1983, 1985), which had been based on measurements of lines at the limit of their sensitivity.

Given the decrease in [Mn/Fe] and [Cr/Fe] values and the accompanying increase in [Co/Fe] and possibly [Ni/Fe], it is natural to infer a shift in iron-peak nucleo-

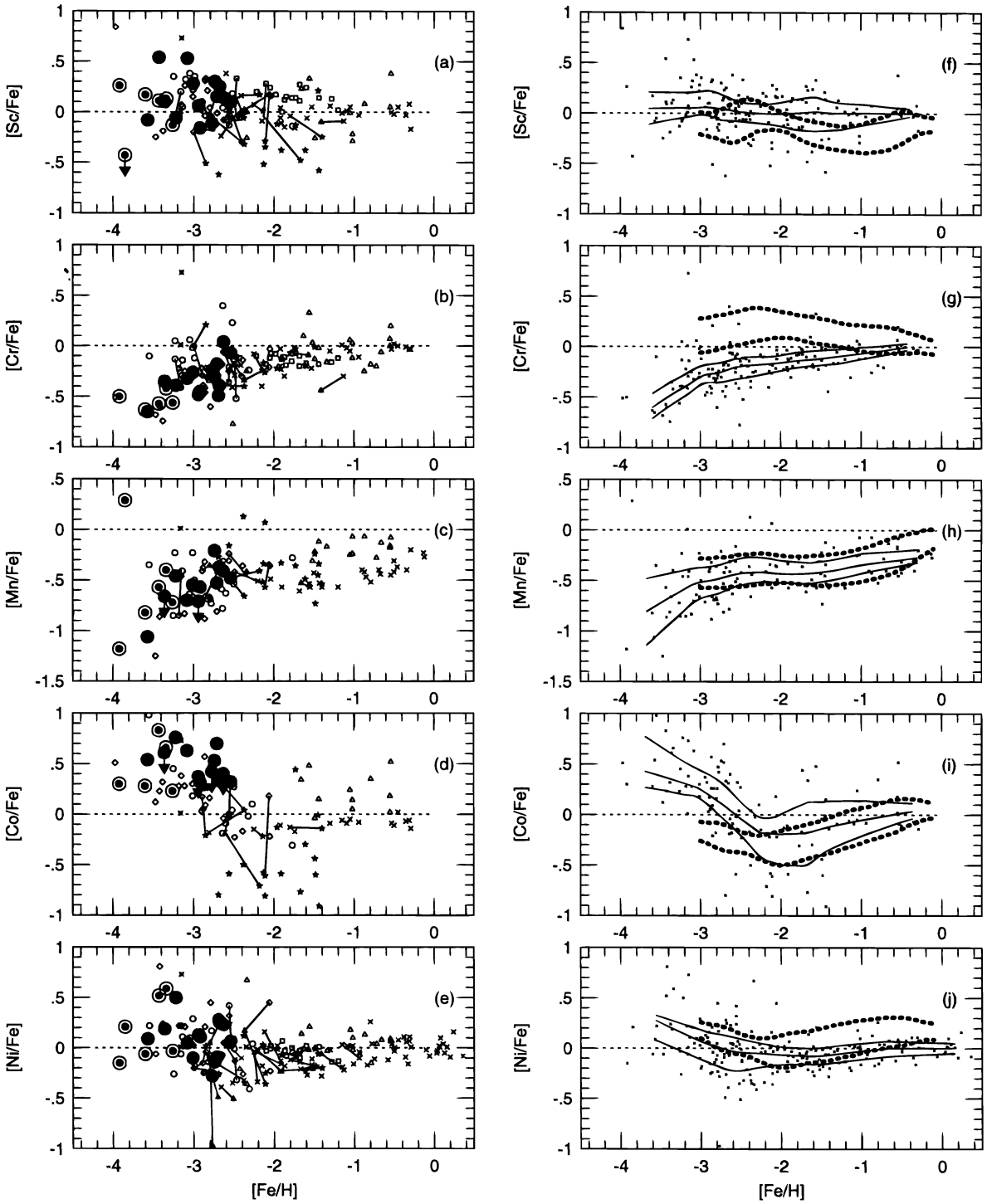

FIG. 4.—Abundances of iron-peak elements in order of increasing atomic number. For Sc, Mn, and Co, upper limits are shown for several stars. See § 5.4 for discussion. Symbols and curves are as in Fig. 2. (*a*) Sc. The low upper limit shown for CS 22876−032 is based on only one line limit and should be verified. (*b*) Cr. (*c*) Mn. The high abundance in CS 22876−032 ([Fe/H] = −3.85, [Mn/Fe] = +0.29) is based on only one observation of one weak line that is probably wrong. (*d*) Co. See § 5.4 for discussion of systematic differences between the data of Gilroy et al. (1988) and others. (*e*) Ni. The three stars with [Fe/H] ∼ −3.3 and [Ni/Fe] ∼ +0.5 are CS 22968−014, CS 22897−008, and CS 22943−137.

synthesis toward higher mass numbers, as suggested by McWilliam et al., who pointed to the α-rich freezeout (Woosley & Hoffman 1992) as a possible culprit. They also noted the general agreement with the behavior of the low-abundance ends of the Timmes et al. (1995) Galactic chemical evolution calculations. Mn and Co have only a single stable isotope each, so we have checked their relative production factors in the nucleosynthetic calculations of Woosley & Weaver (1995) to see if we could identify which stars might be responsible for the altered iron-group elemental abundance ratios. The zero-metallicity SN models of 35 and 40 $M_\odot$ provide similar [Co/Mn] ratios to the higher metallicity models of corresponding mass, but the 22 and 30 $M_\odot$ models of zero metallicity produce much higher

[Co/Mn] ratios (by ~ 1 dex) than at higher metallicities. Since the more massive stars have greater difficulty exploding, one might believe that, of the stars forming from primordial ($Z = 0$) material, only those with $M < 30\ M_\odot$ were capable of enriching the proto-Galactic gas. In that case, one would expect the first enrichment episodes to provide higher [Co/Mn] ratios than later in the halo formation process, as observed.

One of the important goals for those working in the fields of supernovae and metal-poor stars is the desire to understand in detail the nature of the first stars to pollute the proto-Galactic gas. However, it should be borne in mind that the SN models are simplifications of the real events, with three-dimensional calculations and possible effects of rotation and magnetic fields, for example, currently set aside and the explosion mechanism itself treated only approximately. The uncertainties, particularly (but not solely) in the details of the explosion, are probably so great that it would be reading too much into the yields currently available to seriously attempt to link SNs of a particular mass to given observed abundances. The yields from nuclear statistical equilibrium processes occurring close to the mass cut of SNs are especially difficult to predict; the 0.01 $Z_\odot$, 35 $M_\odot$ SNs of Woosley & Weaver produce [Co/Mn] ratios that differ by 0.9 dex depending on whether their explosive treatment "B" or "C" is used, both of which require greater energy that their standard treatment ("A").

Several additional comments on Figure 4 are required. The low upper limit for [Sc/Fe] in CS 22876−032 is based on only one line at a limit of 12 mÅ and should be verified at higher S/N before too much is made of it. However, we recall the discussion earlier about elevated [Al/Fe] and low [Si/Fe] and [Ca/Fe] values for this star. A strong cautionary note is necessary about its [Mn/Fe] value, which is based on only one measurement and is almost certainly wrong; otherwise the star would be astonishingly overabundant in Mn. Upper limits are shown for two stars in [Mn/Fe], which are already low compared with the other stars in the sample, and for four stars in [Co/Fe], which temper the rate at which the [Co/Fe] overabundance can climb. Very large systematic errors are apparent in the Co data, with those of Gilroy et al. (1988) falling considerably below the other studies. The reason for the difference is unclear, but given the high-quality data acquired by Gratton & Sneden (1991) and the small dispersion exhibited by their abundances, we do not favor Gilroy et al.'s result.

5.5. *The Neutron-Capture Elements*

Table 2 presents data on strontium, yttrium, zirconium, barium, and europium. For Zr and Eu, only two detections were made, so we do not plot these elements. The other neutron-capture elements are shown in Figure 5.

5.5.1. *The* [Sr/Fe] *Spread*

Strontium shows the huge spread in relative abundance in very metal-poor stars to which we have become accustomed. We unreservedly reject any suggestion that the abundance range seen for this element in extremely metal-poor stars may be due to observational error. The range in abundance derived for this element, greater than a factor of 100, cannot possibly be explained by errors in the analysis, which should reach at worst a few times 0.1 dex (see Table 3). Inspection of the spectra shown by Ryan et al. (1991, Fig. 11), Norris et al. (1993, Fig. 6), McWilliam et al. (1995a, Fig. 16*a*), and in Paper I (Fig. 1*b*) shows that the differences in line strength from star to star far exceed the noise in the spectra. Baraffe & Takahashi (1993) expressed particular concern, citing the study by Gratton & Sneden (1994), that different Sr lines yield different abundances. While such problems are regrettably common for some elements, such as Al, almost all Sr analyses of stars with [Fe/H] < -3.0 have utilized the Sr II resonance lines since the others become unusably weak. Consequently, the huge scatter in abundances seen in these stars is based on measurements of the same line set; line-to-line differences are not an issue.[8] In further support of the spread seen for Sr, we note that the published abundances are usually based on both Sr II resonance lines, not just one, and these two lines are usually in excellent agreement.

Nevertheless, some cautions must be given. The comments of Baraffe & Takahashi echo our warnings about overinterpreting trends with metallicity when these *are* accompanied by changes in the line list. It is also worth remembering that the solar abundance is seldom derived from the same line set as is used in the study of metal-poor stars, and when it is, it is subject to different radiative transfer conditions. The discordant observations of CS 22891−209 (at [Fe/H] = −3.2) by Primas et al. (1994) and McWilliam et al. (1995b) used the same lines but recorded equivalent widths different by 40–50 mÅ, which for these saturated lines leads to excessive errors. Both groups worked with spectra having the same S/N, so a priori there is no obvious reason to favor one data set over the other. Their measurements for most other elements are in good agreement. The highest [Sr/Fe] value among our sample is for CS 29527−015. This value is noted as uncertain in the table because the two lines yield abundances that differ by 0.7 dex. Rejection of the stronger line would reduce the stated abundance by half this amount. The line pairs in the other stars were in excellent agreement. For an element as heavy as Sr, the thermal broadening is minimal, so microturbulence is much more important than for lighter elements such as iron. Errors in the equivalent widths and microturbulence can change the [Sr/Fe] ratio by ~ 0.1 dex or so.

Equally strongly, we can rule out any suggestion that the Sr abundance variations are restricted to a narrow range of evolutionary types, as might be expected if some phenomenon associated with the host star was responsible for generating the peculiarity. Although most recent studies have involved metal-poor giants from the Beers et al. (1985, 1992b) survey, we remind readers that [Sr/Fe] variations by more than 1 dex at [Fe/H] < -3 originally came to light through the study of main-sequence turnoff stars (Ryan et al. 1991) rather than giants. High-[Sr/Fe] and low-[Sr/Fe] stars are found among both evolutionary types and do not appear to be accompanied by any other chemical peculiarity, lending support to the original suggestion that these stars reflect the range of Sr abundances of the material from which they formed and that the large range seen at a given [Fe/H] attests to inhomogeneous conditions at the time(s) these stars formed.

We note with regard to chemical peculiarities that the lithium abundances in the two original Sr-weak dwarfs are

[8] We note that we have used the Sr II 4215 Å line results of Gratton & Sneden (1994) in Fig. 5.

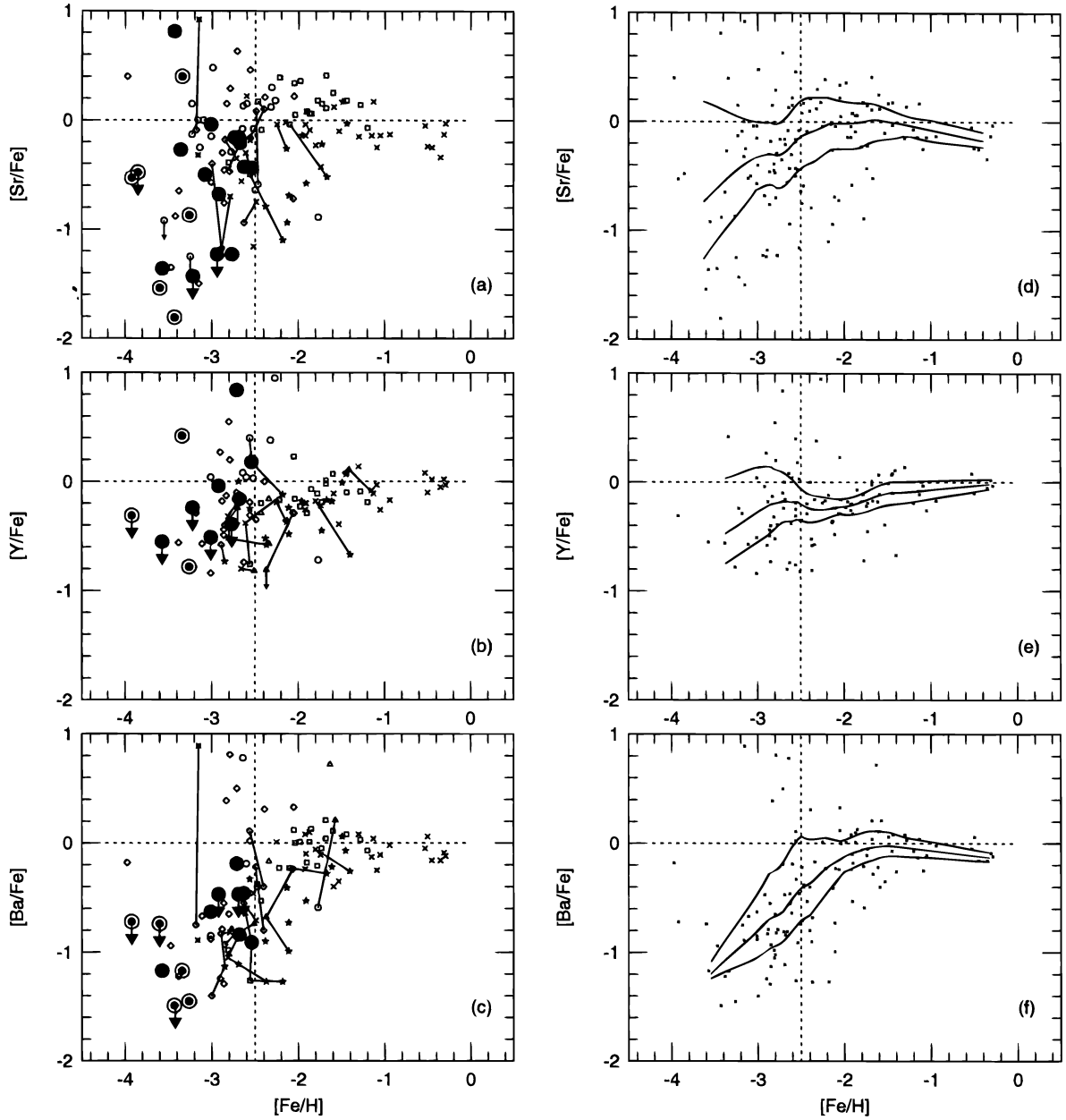

FIG. 5.—Neutron-capture elements. Vertical dotted lines divide the sample at [Fe/H] = −2.50; the more metal-poor sample is reexamined in Fig. 6. Symbols and curves are as in Fig. 2. CS 22897−008 stands out in (*a*) and (*b*), with abundances (from Table 2) [Fe/H] = −3.34, [Sr/Fe] = +0.40, [Y/Fe] = +0.42, and [Ba/Fe] = −1.17; see text for discussion of this star.

typical of most other low-metallicity turnoff stars (Spite & Spite 1993; Norris, Ryan, & Stringfellow 1994). If these stars had undergone some unusual surface disturbance as a result of self-mixing or the dumping of processed material onto their surfaces from companions, one might expect the surface abundance of Li to have undergone modification. Lithium is fragile and easily destroyed if mixed to deeper layers in the star, where temperatures exceed a few million kelvins. The data on Li in CH subgiants are currently rather sparse, but it is possible to point to cases in which the Li abundances range both higher and lower than in otherwise similar halo stars (Ryan et al. 1996). Those with higher Li abundances presumably arise because additional Li has been produced in the AGB companions before being dumped onto the stars now observed. However, in LP 706−7, a CH-strong proper-motion star that we discuss in Paper IV, the Li abundance appears normal, and Thorburn & Beers (1992) reported a Li excess in another CH subgiant, CS 22898−027. Thus the apparent normality of Li in the Sr-poor stars is suggestive, but not on its own convincing, evidence that they have not experienced major modifications of their surface abundance. We speculate that the issue of Li processing in CH-strong stars may be clarified if those currently flagged as CH subgiants on the basis of photometry or strong CH bands are in fact found to encompass stars with more than one origin. Already, McWilliam et al. (1995a) have made the case that CS 22952−052, which might be classified as a CH star on account of its strong CH bands and high neutron-capture element abundances, is in reality a star exhibiting C enrich-

ment and *r*-process patterns from a particular low-mass Type II SN and is not a CH subgiant in the sense of being analogous to the Population I Ba stars. We address issues such as this in Papers III and IV, and we repeat that our deferral of some stars to Paper IV is on the basis of morphology, specifically strong CH-band strength, rather than with a preconceived view of their astrophysical origin.

5.5.2. *Other Neutron-Capture Elements and Comparison with* Sr

It is difficult to learn much from the yttrium abundances. Most studies have investigated different spectral lines, and these yield systematically different results. For most of the extremely metal-poor stars, only upper limits were obtained.

The situation is somewhat better for Ba, with measurable lines in most giants, but whereas McWilliam et al. have studied solely giants, half of our sample are dwarfs, which, being hotter and of higher gravity, have generally weaker line strengths. Consequently, many of the neutron-capture element lines are too weak for us to measure in this evolutionary class. We note two more features of our study. We have deferred discussion of the carbon-rich objects to Paper IV, and since these are generally overabundant in neutron-capture elements, some of the more extreme data presented by McWilliam et al. (1995a) are absent from our Figure 5. Second, the Ba λ4554 measurements of CD $-38°245$ range from detections at 18 and 19 mÅ (Bessell & Norris 1984; Primas et al. 1994) to upper limits of less than 10 and 7 mÅ by Molaro & Castelli (1990) and Peterson & Carney (1989). Our abundance for this star was computed for the conservative datum "less than 20 mÅ."

Since the relative abundances of these two neutron-capture elements might provide insight into the formation process and nucleosynthetic site responsible, we examined them more closely. Unfortunately, most extremely metal-poor dwarfs do not have detections of both Sr and Ba; renewed effort to obtain detections of these important elements will be a task for 8 m telescopes capable of delivering the high S/N required for these faint stars. We note that an extremely metal-poor dwarf with $T_{\rm eff}$/log g/[Fe/H]/ξ = 6000/4.0/$-$4/1 and solar [Sr/Fe] and [Ba/Fe] ratios would have equivalent widths Sr λ4077 = 22 mÅ and Ba λ4554 = 3.1 mÅ.

The scatter evident in Figure 5*c* for [Ba/Fe] is quite different from that in Figure 5*a* for [Sr/Fe]. The spread in [Sr/Fe] at a given [Fe/H] is broad and continuous. However, whereas the total *range* in [Ba/Fe] is almost the same at [Fe/H] = -2.8, the *distribution* in [Ba/Fe] is bimodal, comprising a major trend for stars with [Ba/Fe] < 0 and a few scattered points at [Ba/Fe] > 0. The different behavior of the USMM and LSMM curves for [Sr/Fe] in Figure 5*d*, on the one hand, and for [Ba/Fe] in Figure 5*f* on the other, reemphasize this point.

In Figure 6, for stars with [Fe/H] < -2.5, we present "stripe plots" of the residuals Δ[Sr/Fe], Δ[Y/Fe], and Δ[Ba/Fe], which measure the difference Δ[X/Fe] = [X/Fe]$_*$ $-$ [X/Fe]$_{\rm trend}$ about the trends lines of Figures 5*d*–5*f*. Stripe plots avoid the detrimental effects of binning that occur with histograms, though the latter are also shown. Numerous statistical tests were applied to determine the significance of the bimodality inferred for Ba: (1) All three distributions exhibit at least mild asymmetry, but that for Δ[Ba/Fe] failed the normality tests of Beers et al. (1990b) and had high asymmetry indices (Bird & Beers 1993), in all cases at highly significant levels (better than 0.01). (2) A gap analysis (see, e.g., Beers et al. 1991), utilizing the simulation results of Waines & Schacht (1978), identified no significant gaps in the Δ[Sr/Fe] and Δ[Y/Fe] distributions but found two in the Δ[Ba/Fe] residuals, at the locations indicated by asterisks in Figure 6*c*. These have "per gap" probabilities 0.006 and 0.0005 for the smaller and larger gaps, respectively, and a "total gap" probability of 0.02. The former indicates that the gaps are too large at their identified location to be consistent with sampling of a Gaussian parent population, and the latter that two gaps this large should not be found anywhere in a Gaussian parent. (3) A mixture model analysis (see, e.g., Beers et al. 1992a) using the KMM algorithm described by Ashman, Bird, & Zepf (1994), indicated no significant partitions in the Δ[Sr/Fe] and Δ[Y/Fe] distributions but found a highly significant split for Δ[Ba/Fe]. Irrespective of whether the dispersions of the two Ba groups were forced to be equal or allowed to differ, the analysis identified two groups centered at Δ[Ba/Fe] = 0.0 and +1.4, containing 26 and seven stars, respectively, each with a dispersion of 0.3 dex.

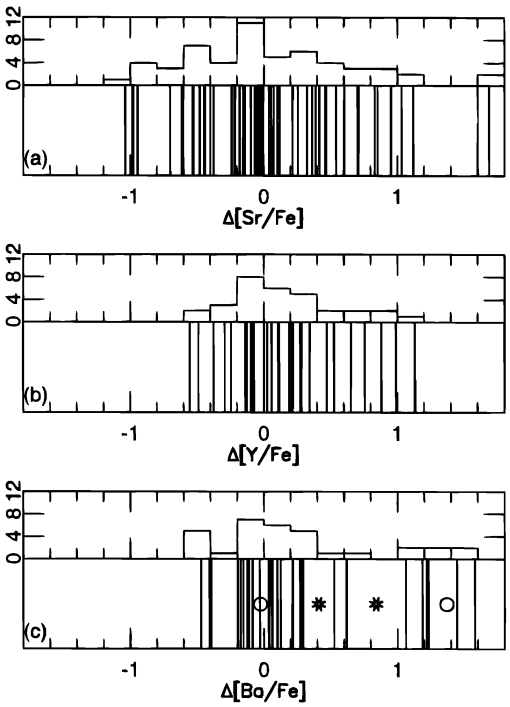

FIG. 6.—Stripe plots for residuals of (*a*) [Sr/Fe], (*b*) [Y/Fe], and (*c*) [Ba/Fe] about the trend lines in Figs. 5*d*–5*f*, for stars with [Fe/H] < -2.5. Stripe plots show the distribution of residuals without the detrimental effects of binning that occurs in histograms, though the latter are also shown for convenience. The asterisks in (*c*) indicate the locations of the statistically significant gaps identified in the "gap analysis"; see discussion in § 5.5.2. The circles indicate the centers of the two components highlighted by the mixture-model analysis.

The conclusion from these analyses is that the [Ba/Fe] residuals are unquestionably bimodal. If the scatter in [Ba/Fe] were due to some process describable by a continuous range of parameters, a spread resembling that for [Sr/Fe] would be expected. That [Ba/Fe] has a much smaller scatter about its major trend plus a handful of *separated* high points leads us to conclude that the high-[Ba/Fe] data points have a different origin from the majority of the barium data. What has yet to be determined is

whether that bimodality is astrophysical in origin or results from non-Gaussian systematic errors in some of the data, but closer examination of the stars with [Ba/Fe] > 0 seems warranted.

In Figure 7, we show [Ba/Fe] versus [Sr/Fe] for stars with [Fe/H] ≤ -2.50. This abundance range is further subdivided into the metallicity ranges $-2.80 < [Fe/H] \leq -2.50$, $-3.20 < [Fe/H] \leq -2.80$, and [Fe/H] ≤ -3.20. We show two lines drawn through the solar abundance point, having slopes 1.0 and 2.0. The data are scattered about some overall trend, which, as far as one can tell given the scatter and the large intrinsic spread in [Sr/Fe] at [Fe/H] < -3.2, suggests that strontium and barium vary roughly equally relative to iron for low abundance ratios, but with the possibility that [Ba/Fe] changes faster than [Sr/Fe] for those stars with [Ba/Fe] > 0. We note, however, that this latter group contains precisely those we identified in the previous paragraph as being *separate* from, not just scattered above, the major [Ba/Fe] versus [Fe/H] trend. It is clearly of interest to confirm whether their [Ba/Fe] ratios are reliable and, if so, why these stars differ from "normal" metal-poor stars.

The star that stands out most in Figure 7*d* is CS 22897−008, with [Sr/Fe] = 0.4 and [Ba/Fe] = −1.2. McWilliam et al. (1995a) also noted its high [Sr/Ba] value. We point out that the yttrium abundance of CS 22897−008 (based on six lines) is also very high (Fig. 5*b*). These observations suggest that the light neutron-capture elements have been produced considerably more abundantly than heavier nuclei. One means by which this can occur, as appreciated by McWilliam et al., is the "weak" *s*-process, which acts during core He burning of $M > 15\ M_\odot$ stars and produces neutron-capture elements only between Cu and Zr. A large contribution from the weak *s*-process might explain the unusual [Sr/Ba] and [Y/Ba] ratios in this star. Although Baraffe & Takahashi (1993) found this process incapable of producing the high *absolute* abundances observed in the halo population, it might be possible for a star forming from poorly mixed gas in which weak-*s* products existed. One often associates neutron-capture elements in the halo with the *r*-process (e.g., Truran 1981; Sneden & Parthasarathy 1983), though Mathews, Bazan, & Cowan (1992) have shown that *s*-processing with a primary neutron source in 1–7 $M_\odot$ may be responsible. (See also Magain 1995 for a view opposing an *r*-process interpretation.) Mathews et al. also discussed *r*-processing in low-mass (7–8 $M_\odot$) stars as a viable source of the observed abundances. It is interesting that Woosley et al. (1994) found "unacceptable overproduction" of the dominant isotopes of Sr, Y, and Zr in their *r*-process calculations. Our analysis of the G band of this star with the techniques described in Paper IV shows it to be also overabundant in carbon, with [C/Fe] = +0.6 dex. This result compares favorably with McWilliam et al.'s [C/Fe] = +0.34 dex. Although these values are not high enough to promote it into the same category as stars like CS 22892−052, it is at least 2–4 times more abundant in C than "normal" metal-poor giants. The overabundance of both C and neutron-capture elements is not surprising, given their joint production in AGB stars and their possible production in stars toward the lower end of the Type II SN mass range, such as the 10–11 $M_\odot$ site of the *r*-process considered by Mathews & Cowan (1990) as an explanation for the decline of Eu (*r*-process) abundances in the most metal-poor stars.

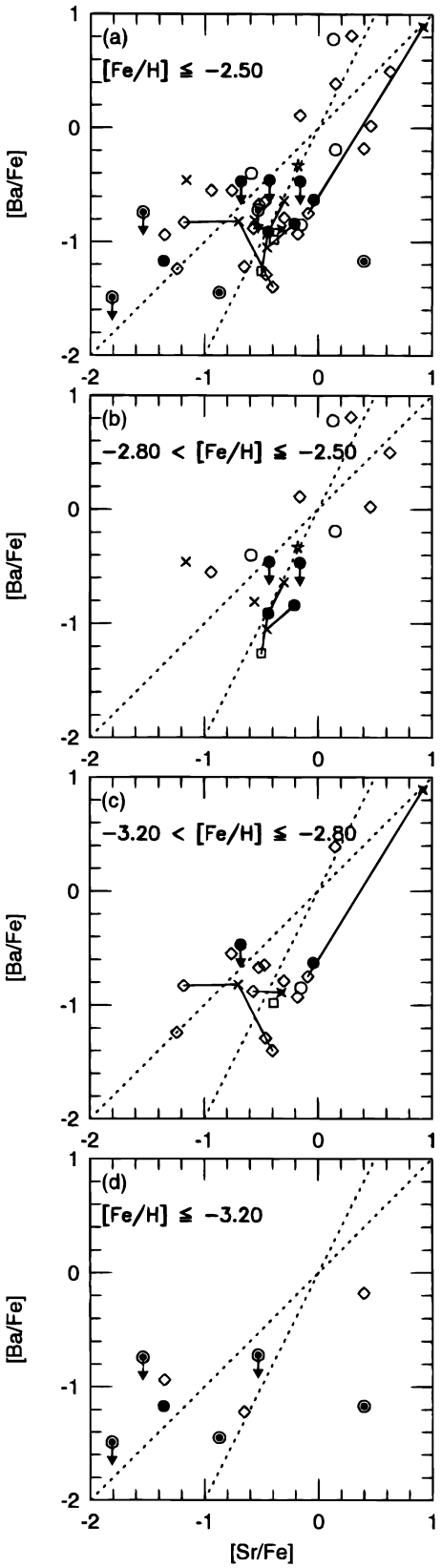

FIG. 7.—(*a*) [Ba/Fe] ratio vs. [Sr/Fe] for stars having [Fe/H] ≤ -2.50. (*b–d*) The sample in (*a*) further subdivided into three smaller metallicity ranges, as indicated. Two dashed lines are drawn through the solar abundance point with slopes 1.0 and 2.0; see § 5.5.2 for discussion. CS 22897−008 stands out in (*a*) and (*d*), with abundances (from Table 2) [Sr/Fe] = +0.40 and [Ba/Fe] = −1.17; see text for discussion of this star. Symbols are as in Fig. 2.

Given CS 22892−052's *r*-process rather than *s*-process signature, McWilliam et al. prefer to associate it with such lower mass Type II SNs rather than with AGB ejecta.

5.6. *How Did the First Supernovae Pollute Their Environments?*

We can also learn from extremely metal-poor stars about the onset of chemical evolution in the Galaxy. The well-defined abundance trends seen in the halo contrast with the Searle & Zinn (1978) view of a very chaotic halo-formation mechanism, with independently evolving fragments coalescing into the modern Galactic halo over a period on the order of 10^9 yr, exceeding the lifetimes of the enriching SN progenitors by several orders of magnitude. McWilliam et al. (1995a) discussed several aspects of this, including options for metallicity-dependent yields.

One deficiency of current Galactic chemical evolution models is that, although nucleosynthetic yields are used to provide relative abundances for the elements, the details of how they are mixed into the environment are generally overlooked. It is often assumed that one cloud, having the mass of the halo or even the mass of the Galaxy (rather than independently evolving halo clouds as Searle & Zinn envisaged) is enriched by numerous supernovae conforming to an adopted initial mass function, and the products of these are completely mixed into the cloud. While such a model should serve well in the Galactic disk and perhaps at late times during formation of the halo, it is unlikely to be applicable earlier in the formation of the halo, when the gas clouds were poorly mixed, independently evolving, and have been contaminated by only very small numbers of SNs. In the remaining paragraphs, we examine this aspect of chemical evolution in greater detail.

5.6.1. *Enrichment Independent of Cloud Size and Density*

Recall from Timmes et al. (1995) that at [Fe/H] < -2.5 the effects of massive supernovae dominate, where "massive" means between 30 $M_\odot$ and the limit for complete collapse to a black hole. The protohalo was sufficiently poorly mixed in this epoch that ranges $\gtrsim 100$ in [Sr/Fe] were not evened out. Audouze & Silk (1995) present mixing and timing arguments to deduce that at most two to three SNs could have contributed to the enrichment of a particular cloud at this epoch, consistent with Ryan et al.'s (1991) conclusion, from both the enrichment capability of SNs and from the disappearance of Sr in some stars, that some of the stars observed at [Fe/H] < -3 are only second-generation stars. The abundance patterns, especially those of Cr, Mn, and Co, raise the following question: why should all halo supernovae ejecta around this epoch that possess a particular [Cr/Fe] ratio (or [Mn/Fe] or [Co/Fe] ratio) *subsequently* form into stars of the same [Fe/H]? Put differently, how do the ejecta know how much interstellar hydrogen to combine with? Nature seems to require that the ejecta of two SNs producing identical [Cr/Fe] ratios combine with identical environmental gas masses. The permitted range in mass would be a factor less than 10, based on the narrow range in [Fe/H] spanned at a given [Cr/Fe].

If metal-poor, massive star formation is triggered at some critical cloud density, then the star-forming clouds may be essentially identical in the vicinity (and over the short lifetime) of massive SNs. Two identical SNs would then be expected to produce similar degrees of metal enrichment in the next stellar generation since their environments would be almost the same. However, if the star-forming clouds are not all very similar, then an alternative is required.

As an alternative, we argue that the mixable cloud mass may be set by the kinetic energy of the ejected SN layers. It seems reasonable that a given *mass* of ambient gas is required to brake ejecta of a given energy, largely independently of the density or total mass of the cloud; the more energy deposited, the greater the mass of ISM gas required to dissipate that energy and assimilate the ejecta. This supposition receives theoretical support from the work of Cioffi, McKee, & Bertschinger (1988) on the evolution of supernova remnants (SNRs, as opposed to stellar remnants). Their analytic expressions (4.4b) and (3.33a) give the radius of a supernova remnant when it merges with the ambient interstellar medium. Converting this to a volume and multiplying by the ambient density, we obtain the mass of the ISM mixed with the ejecta:

$$m_{\rm ISM} = 3.4 \times 10^4 E_{51}^{0.95} n_0^{-0.10} \zeta_m^{-0.15} (\beta C_{06})^{-1.29}\ M_\odot\ ,$$

where E_{51} is the SN energy in units of 10^{51} ergs, n_0 is the number density of hydrogen in the ambient ISM per cubic centimeter, ζ_m is the ISM metallicity in solar units, and βC_{06} is the ISM isothermal sound speed in units of 10^6 cm s^{-1} multiplied by a factor β that indicates by how much the shock velocity exceeds the sound speed. Merging of the remnant with the ISM occurs when β attains a value of order unity. Consistent with our "hand-waving" argument, we find from Cioffi et al.'s work that the mixable mass of the ISM depends *only very weakly* on the cloud conditions, varying roughly as the -0.1 power of the density and metallicity, but depends essentially *linearly* on the energy of the ejecta.[9] Thus, regardless of the size or density of the cloud into which the first SNs explode, we expect similar cloud masses to be polluted by SNs of similar energy. Since the iron-peak nuclei are produced near the mass cut, it is not unreasonable that SNs producing the same iron-group elemental ratios should impart the same kinetic energy to their envelopes. This energy could vary with stellar mass, metallicity, or both, and the protohalo cloud masses and densities could vary greatly, but the tight abundance correlation observed would still be obtained, provided the iron-group yields correlated with explosive energy. Effectively, this scenario sees the environmental enrichments dependent upon a universal property, namely, SN physics, rather than on the details of the environment itself, despite diverse cloud sizes and densities.

5.6.2. *Synchronized Abundances despite Chaotic Dynamics*

In this scenario, massive, low-metallicity stars form and explode as SNs to enrich bubbles embedded within protohalo clouds, independent of one another as expected from the huge distances and short time for dynamical evolution. However, the resulting chemical enrichment of the gas surrounding these separately evolving systems is forced to resemble that from identical supernovae elsewhere by the

[9] It is not clear whether the assumptions underlying this model will be valid at the low metallicity of the protohalo, but given the very small dependence on metallicity, we expect the abundance-related effects to be minimal. One might also be concerned about Cioffi et al.'s assumption of uniform density in the surrounding cloud since the ISM is far from uniform. However, since the mass depends only very weakly on density between environments, it is probably safe to expect little dependence on inhomogeneities within an environment. Density nonuniformities may, however, result in nonuniform mixing of the ejecta within the SNR.

energetics of the explosions and the gas mass required to brake the expansion. Thorough mixing would be expected *within* any SNR, but not *between* bubbles. The protohalo clouds may be many in number and evolving separately from the others, but the chemical patterns would still be synchronized by the physics of the SN explosions, even though the protohalo clouds evolve independently, at different times and in different parts of what we now call the Galactic halo. Such a picture would remain consistent with both the well-defined abundance patterns seen in very metal-poor stars and the lack of kinematic correlations with abundance, which prompted Searle & Zinn (1978) to propose a protracted, nonuniform period for the formation of the Galactic halo.

5.6.3. *The Minimum Metallicity for Globular Clusters and Their Chemical Homogeneity*

The formulation above showed that the mass of interstellar medium polluted by a SN depends on the SN's energy but is essentially independent of the density (or dimensions) of the cloud. We note with interest another result, emerging from a quantitative assessment of what the polluted mass is. Adopting energy 1×10^{51} ergs, density 0.1 cm^{-3}, $C_{06} = 1$, and $\beta = 2$ from Cioffi et al., and considering a metallicity $10^{-4}\ Z_{\odot}$, we compute that typically $m_{ISM} = 7 \times 10^4\ M_{\odot}$. We emphasize that since the density and metallicity enter the relation with very small powers (-0.10 and -0.15, respectively), changes by a factor of 1000 in either of these parameters will only bring about less than a factor of 3 change in the polluted mass. The cloud parameter that most affects the calculation is the sound speed, which varies as the square root of the temperature. Allen (1973, § 126) suggested a temperature range of a factor of 3 for H I regions, leading to a cloud mass variation factor of 2. We note further that use of Allen's (§ 22) value for C_{06} in interstellar H I, 0.16, would increase the mass estimate by a factor of 11 to $8 \times 10^5\ M_{\odot}$.

Woosley & Weaver's (1995) $Z = 10^{-4}\ Z_{\odot}$, 25 $M_{\odot}$ supernova model "U25A" expels (from their final production factors) 0.213 $M_{\odot}$ of iron. Mixing this into a $7 \times 10^4\ M_{\odot}$ bubble of primordial ISM would result in [Fe/H] $= -2.7$ within this region. Cioffi et al. noted that the ejecta and ISM are fully mixed within the SNR, though we speculate that the mixing may be nonuniform in a cloud of nonuniform density. We note that this abundance coincides (approximately) with:

1. The occurrence of the change in iron-group elemental abundance patterns, as highlighted by McWilliam et al. (1995a) and supported by our own data (Fig. 4);
2. The lowest metallicity for Galactic globular clusters, whereas halo field stars extend to lower metallicities (e.g., Ryan & Norris 1991b); and
3. The onset of huge ($\gtrsim$2 dex) ranges in [Sr/Fe];

and also that this abundance is consistent with Timmes et al.'s (1995) "problem" that at [Fe/H] ≤ -2.5 the effects of uncertainties in massive-star nucleosynthesis were showing, which would be less likely if many SNs were contributing to their tallies at that epoch.

Present-day globular cluster masses range from 10^4 to $10^6\ M_{\odot}$. The polluted mass calculated above ($7 \times 10^4\ M_{\odot}$) is comparable with the lower range of these values, and it is perhaps more than coincidence that the metallicity predicted in the wake of one SNR matches the lowest metallicity found for globular clusters in the Galaxy.[10] The internal chemical homogeneity of the smallest clusters would arise naturally if only one or at most a few overlapping SNRs have been responsible for the enrichment of each one. It would also explain why large abundance inhomogeneities seem more common in the more massive systems such as ω Cen (see, e.g., Norris & Da Costa 1995) since larger numbers of SNs would be required to enrich these larger clouds, leading to greater probability of diverse products and incomplete mixing between only partially overlapping or nonoverlapping SNRs.

5.6.4. *Abundance Diversity in Metal-poor Field Halo Stars*

Just as the metallicity predicted for the "typical" SNR matches the lowest metallicity found for globular clusters, it also matches the metallicity below which very different abundance patterns are seen in the halo field stars, as seen in Figures 2–6. Field stars may have formed in less tightly bound clouds that were more readily broken up than the globular clusters, and in which the star formation rate would be lower. In such an environment, weak enrichment events due to SNs that can barely shed their outer layers are less likely to be overshadowed by the ejecta of "typical" SN enrichments. It is not surprising, therefore, that below [Fe/H] $\simeq -2.7$ we should see more diverse abundance ratios, and second that we should see stars of this low metallicity at all whereas, in more tightly bound, more massive clouds, there is greater probability that one or at most a few "typical" SNs will set the lower limit on that cloud's metallicity and, consequently, the metallicity of the surviving cluster.

6. CONCLUSIONS

6.1. *Procedures and Comparisons*

We have obtained spectra of 23 very metal-poor dwarfs and giants. Equivalent widths were presented in Paper I. In the present paper, we analyze 19 of these to derive abundances for elements between Mg and Eu. All have [Fe/H] < -2.5, and 10 have [Fe/H] < -3.0. In addition, for six stars with [Fe/H] < -3.0, we compile and analyze equivalent width measurements from the literature (including our own data).

We perform an LTE analysis, though for Al we cite Baumueller & Gehren's (1996, private communication) NLTE calculations, which require an upward revision of dwarf abundances from the 3961 Å line by 0.4 to 0.6 dex. Hyperfine effects are computed for Mn and Co. We endeavor to use laboratory *gf*-values; only on rare occasions are solar *gf*-values used. Surface gravities are obtained from the Fe I–to–Fe II ionization balance, provided more than one or two ionized lines were measured.

We compare our analysis and results closely with those of McWilliam et al. (1995a), who studied very metal-poor giants. We conclude that any differences between our analysis and McWilliam et al.'s will be (1) systematic, (2)

[10] The mass agreement may be strained, however, if 90% of the SNR mass must be "lost" from the system. Mass loss of this order from halo star formation has been suggested by Hartwick (1976) among others, though whether the gas is physically removed or just made too hot to form stars is uncertain. It is not clear whether the SNR mass would be affected in this way. The mass objection would vanish if the lower sound speed were used since this increases the cloud mass by a factor of 11, but then the ejecta would be diluted to [Fe/H] $= -3.7$.

confined to lines stronger than 100 mÅ, and (3) even then will be less than 0.1 dex. The good agreement in the abundances we derive for stars in common supports this conclusion.

We also undertake a statistical analysis of the [X/Fe] versus [Fe/H] diagrams, using robust statistical techniques to compute and show the major trends in the elemental abundances, and then compare these with the predictions of a Galactic chemical evolution model (Timmes et al. 1995).

6.2. *Elemental Abundances*

The sample is presented in Table 1. Our adopted effective temperatures are higher by up to 250 K than in previous studies because of the color–effective temperature scale we have used. Our abundances are in excellent agreement with previous determinations, modulo this temperature difference.

The lowest abundance we derive for a previously unobserved star is [Fe/H] = −3.57, for CS 22172−002. Adopting the solar abundance log $(N(\mathrm{Fe})/N(\mathrm{H})) = -4.50$, we now identify six stars with [Fe/H] < −3.50 from high-resolution analyses. (We specifically exclude post–AGB binaries that have lost their least volatile elements onto grains, and C-rich stars, from this tally.) Elemental abundances are listed in Table 2.

The α-elements Mg, Si, and Ca continue their almost uniform overabundances seen in more metal-rich halo stars down to at least [Fe/H] = −4. [Mg/Fe] increases slightly at [Fe/H] < −2.5, but the slope is shallow and could be due to systematics in the analysis. Titanium also continues its overabundance down to at least [Fe/H] = −4. It is difficult to avoid the conclusion that it is produced abundantly in massive stars and in uniform proportion to the α-elements, even though stellar nucleosynthetic calculations do not predict this behavior.

The plateau in [Al/Fe] = −0.8, which is reached by our stars with [Fe/H] < −2.5, extends at least down to [Fe/H] = −4. However, Baumueller & Gehren (1996, private communication) calculate that LTE abundances for the resonance lines must be corrected upward by 0.4 to 0.6 dex, at least for dwarfs, in which case the plateau lies nearer [Al/Fe] = −0.3. This level is still well below [Mg/Fe], consistent with an odd-even effect. Moreover, Timmes et al. (1995) predicted this value, apparently without knowledge of the NLTE corrections. CS 22949−037, discussed extensively by McWilliam et al. (1995a), and CS 22876−032 have [Al/Fe] above the plateau but [Al/Mg] nearer the mean trend. They appear to show real variations in elemental yields, with the light elements Al and Mg produced in their normal ratios to one another, but with CS 22876−032 depressed in [Si/Fe], [Ca/Fe], and possibly [Sc/Fe].

We confirm McWilliam et al.'s (1995a) discovery that, at [Fe/H] < −2.5, the light iron-group elements Cr and Mn become more underabundant than at higher metallicity and that the heavy iron-group element Co becomes overabundant, and we extend the result to dwarfs as well as giants. We also point to an overabundance in [Ni/Fe] in *some* of the lowest metallicity stars, but we question whether this mean overabundance is dominated by just a few stars rather than delineating an overall trend. For several elements, real star-to-star abundance differences appear common at the lowest metallicities.

[Sr/Fe] shows a spread $\gtrsim$2 dex at [Fe/H] < −3, exceeding all reasonable errors in the observations and analysis. This spread exists for both dwarfs and giants and is not confined to some narrow range of evolutionary types as might be expected if it were created by some process occurring in the observed stars themselves. Ba, on the other hand, exhibits considerably less scatter, showing a well-defined decrease in [Ba/Fe] as [Fe/H] decreases below −2.0. A small number of stars with [Ba/Fe] > 0 lie well away from the main trend. It is unclear whether they stand apart for astrophysical (i.e., natural) reasons or whether there are problems with their analysis.

CS 22897−008 has high Sr and Y abundances for its [Fe/H], but normal Ba. [C/Fe] is also elevated in this star. The light neutron-capture elements can be produced in the weak *s*-process, though neutron-capture elements seen in metal-poor stars are often, though not universally, assumed to arise by the *r*-process.

It is clear that not all stars at a given [Fe/H] have the same abundance patterns.

6.3. *Galactic Chemical Evolution*

We propose that enrichment of the ISM by the first few SNs depended primarily on the SNs' energy and was essentially independent of the size or density of the clouds in which they exploded. If SN yields in the iron group correlate with explosive energy, which seems reasonable since they form near the mass cut, then the chemical enrichment patterns can maintain their tight correlation (as is observed) despite the protohalo's being poorly mixed (as evidenced by the [Sr/Fe] and other elemental variations) and star formation having occurred in regions widely separated in both space and time (Searle & Zinn 1978).

Using the model of supernova remnants by Cioffi et al. (1988), we calculate that a typical enrichment episode in the newly forming protohalo will produce [Fe/H] = −2.7. This coincides with the observed lower limit to the metallicity of Galactic globular clusters. It also coincides with the metallicity for field halo stars below which greater diversity of abundance ratios in seen, consistent with these stars' having formed in less tightly bound clouds than the globular clusters, subject to weaker enrichment events associated with massive, low-metallicity stars.

The authors are grateful to the Australian Time Assignment Committee for their continued support of this project, and to the director, R. D. Cannon, and staff of the Anglo-Australian Observatory for providing facilities for this study. S. G. R. and J. E. N. express their gratitude to the (Australian) Department of Industry, Science, and Technology for provision of a grant from the Bilateral Science and Technology Collaboration Program, which partially supported this work. S. G. R. was supported by an Australian Research Council Postdoctoral Fellowship during part of this study and gratefully records his thanks to the director of the National Astronomical Observatory (Japan), K. Kodaira, and to T. Kajino, for the provision of a Foreign Research Fellowship, during which time this paper was completed; S. G. R. also enjoyed fruitful discussions with N. Arimoto and K. Nomoto over this period. T. C. B. acknowledges partial support for this work from an All University Research Initiation Grant awarded by Michigan State University, and from grants AST 90-1376, AST 92-22326, and INT 94-17547 awarded by the National Science Foundation.

REFERENCES

Allen, C. W. 1973, Astrophysical Quantities (3d ed.; London: Athlone)
Anders, E., & Grevesse, N. 1989, Geochim. Cosmochim. Acta, 53, 197
Arpigny, C., & Magain, P. 1983, A&A, 127, L7
Ashman, K. A., Bird, C. M., & Zepf, S. E. 1994, AJ, 108, 2348
Audouze, J., & Silk, J. 1995, ApJ, 451, L49
Baraffe, I., & Takahashi, K. 1993, A&A, 280, 476
Barbuy, B., Spite, F., & Spite, M. 1985, A&A, 144, 343
Bard, A., Kock, A., & Kock, M. 1991, A&A, 248, 315
Bard, A., & Kock, M. 1994, A&A, 282, 1014
Beers, T. C., Flynn, K., & Gebhardt, K. 1990a, AJ, 100, 32
Beers, T. C., Forman, W., Huchra, J. P., Jones, C., & Gebhardt, K. 1991, AJ, 102, 1581
Beers, T. C., Gebhardt, K., Huchra, J. P., Forman, W., Jones, C., & Bothun, G. D. 1992a, ApJ, 400, 410
Beers, T. C., Norris, J. E., & Ryan, S. G. 1996, in preparation
Beers, T. C., Preston, G. W., & Shectman, S. A. 1985, AJ, 90, 2089
———. 1992b, AJ, 103, 1987
Beers, T. C., Preston, G. W., Shectman, S. A., & Kage, J. A. 1990b, AJ, 100, 849
Bell, R. A., Eriksson, K., Gustafsson, B., & Nordlund, Å. 1976, A&AS, 23, 37
Bell, R. A., & Gustafsson, B. 1978, A&AS, 34, 229
———. 1989, MNRAS, 236, 653
Bell, R. A., & Oke, J. B. 1986, ApJ, 307, 253
Bessell, M. S., & Norris, J. 1984, ApJ, 285, 622
Biémont, E., Baudoux, M., Kurucz, R. L., Ansbacher, W., & Pinnington, E. H. 1991, A&A, 249, 539
Bird, C. M., & Beers, T. C. 1993, AJ, 105, 1596
Blackwell, D. E., Ibbetson, P. A., Petford, A. D., & Shallis, M. J. 1979a, MNRAS, 186, 633
Blackwell, D. E., Lynas-Gray, A. E., & Smith, G. 1995, A&A, 296, 217
Blackwell, D. E., Petford, A. D., & Shallis, M. J. 1979b, MNRAS, 186, 657
Blackwell, D. E., Petford, A. D., Shallis, M. J., & Simmons, G. J. 1980, MNRAS, 191, 445
———. 1982a, MNRAS, 199, 43
Blackwell, D. E., Petford, A. D., & Simmons, G. J. 1982b, MNRAS, 201, 595
Blackwell, D. E., Smith, G., & Lynas-Gray, A. E. 1995, A&A, 303, 575
Bond, H. E. 1974, ApJ, 194, 95
Booth, A. J., Shallis, M. J., & Wells, M. 1983, MNRAS, 205, 191
Buser, R., & Kurucz, R. L. 1992, A&A, 264, 557
Carney, B. W., Latham, D. W., Laird, J. B., & Aguilar, L. A. 1994, AJ, 107, 2240
Carney, B. W., & Peterson, R. C. 1981, ApJ, 245, 238
Cioffi, D. F., McKee, C. F., & Bertschinger, E. 1988, ApJ, 334, 252
Cleveland, W. S., & Devlin, S. J. 1988, J. Am. Stat. Assoc., 83, 596
Cleveland, W. S., & Kleiner, B. 1975, Technometrics, 17, 447
François, P. 1986, A&A, 160, 264
Froese Fischer, C. 1975, Canadian J. Phys., 53, 184
Fuhr, J. R., Martin, G. A., & Wiese, W. L. 1988, J. Phys. Chem. Ref. Data, 17, suppl. 4
Fuhrmann, K., Axer, M., & Gehren, T. 1994, A&A, 285, 585
Gass, H., Liebert, J., & Wehrse, R. 1988, A&A, 189, 194
Gehren, T., Reile, C., & Steenbock, W. 1991, in Stellar Atmospheres: Beyond Classical Models, ed. L. Crivellari, I. Hubeny, & D. G. Hummer (NATO ASI Ser. C, 341) (Dordrecht: Kluwer), 387
Gilroy, K. K., Sneden, C., Pilachowski, C. A., & Cowan, J. J. 1988, ApJ, 327, 298
Gratton, R. G. 1989, A&A, 208, 171
Gratton, R. G., & Sneden, C. 1987, A&A, 178, 179
———. 1988, A&A, 204, 193
———. 1991, A&A, 241, 501
———. 1994, A&A, 287, 927
Grevesse, N., Blackwell, D. E., & Petford, A. D. 1989, A&A, 208, 157
Gustafsson, B., Bell, R. A., Eriksson, K., & Nordlund, Å. 1975, A&A, 42, 407
Guthöhrlein, G. H., & Keller, H. P. 1990, Z. Phys. D, 17, 181
Hannaford, P., Lowe, R. M., Grevesse, N., & Noels, A. 1992, A&A, 259, 301
Hartwick, F. D. A. 1976, ApJ, 209, 418
Hobbs, L. M., Welty, D. E., & Thorburn, J. A. 1991, ApJ, 373, L47
Holweger, H., Bard, A., Kock, A., & Kock, M. 1991, A&A, 249, 545
Holweger, H., Heise, C., & Kock, M. 1990, A&A, 232, 510
Holweger, H., Kock, M., & Bard, A. 1995, A&A, 296, 233
Kostik, R. I., Shchukina, N. G., & Rutten, R. J. 1996, A&A, 305, 325
Kurucz, R. L. 1993, CD-ROM 13, ATLAS9 Stellar Atmospheres Programs and 2 km/s Grid (Cambridge: Smithsonian Astrophys. Obs.)
Lambert, D. L. 1989, in AIP Conf. Proc. 183, Cosmic Abundances of Matter, ed. C. J. Waddington (New York: AIP), 168
Lambert, D. L., & Luck, R. E. 1978, MNRAS, 183, 79
Luck, R. E., & Bond, H. E. 1981, ApJ, 244, 919
———. 1983, ApJ, 271, L75
———. 1985, ApJS, 59, 249
Magain, P. 1984, A&A, 134, 189
———. 1987, A&A, 179, 176
———. 1988, in IAU Symp. 132, The Impact of Very High S/N Spectroscopy on Stellar Physics, ed. G. Cayrel de Strobel & M. Spite (Dordrecht: Kluwer), 485
———. 1989, A&A, 209, 211
———. 1995, A&A, 297, 686
Mathews, G. J., Bazan, G., & Cowan, J. J. 1992, ApJ, 391, 719
Mathews, G. J., & Cowan, J. J. 1990, Nature, 345, 491
McClure, R. D. 1984, in IAU Symp. 105, Observational Tests of the Stellar Evolution Theory, ed. A. Maeder & A. Renzini (Dordrecht: Reidel), 187
McWilliam, A., Preston, G. W., Sneden, C., & Searle, L. 1995a, AJ, 109, 2757
McWilliam, A., Preston, G. W., Sneden, C., & Shectman, S. 1995b, AJ, 109, 2736
Molaro, P., & Bonifacio, P. 1990, A&A, 236, L5
Molaro, P., & Castelli, F. 1990, A&A, 228, 426
Nissen, P. E. 1989, Messenger, 58, 40
Norris, J. E., & Da Costa, G. S. 1995, ApJ, 447, 680
Norris, J. E., Peterson, R. C., & Beers, T. C. 1993, ApJ, 415, 797
Norris, J. E., Ryan, S. G., & Beers, T. C. 1996a, ApJS, in press (Paper I)
———. 1996b, ApJ, submitted (Paper III)
———. 1996c, in preparation (Paper IV)
———. 1996d, in preparation
Norris, J. E., Ryan, S. G., & Stringfellow, G. S. 1994, ApJ, 423, 386
O'Brian, T. R., Wickliffe, M. E., Lawler, J. E., Whaling, W., & Brault, J. W. 1991, J. Opt. Soc. Am. B, 8, 1185
Peterson, R. C. 1981, ApJ, 244, 989
Peterson, R. C., & Carney, B. W. 1989, ApJ, 347, 266
Peterson, R. C., Kurucz, R. L., & Carney, B. W. 1990, ApJ, 350, 173
Primas, F., Molaro, P., & Castelli, F. 1994, A&A, 290, 885
Ryan, S. G. 1989, AJ, 98, 1693
Ryan, S. G., Beers, T. C., Deliyannis, C. P., & Thorburn, J. A. 1996, ApJ, 458, 543
Ryan, S. G., & Norris, J. E. 1991a, AJ, 101, 1835
———. 1991b, AJ, 101, 1865
Ryan, S. G., Norris, J. E., & Bessell, M. S. 1991, AJ, 102, 303
Schuster, W. J., Nissen, P. E., Parrao, L., Beers, T. C., & Overgaard, L. P. 1996, A&AS, 117, 317
Searle, L., & Zinn, R. 1978, ApJ, 225, 357
Smith, G., & O'Neill, J. A. 1975, A&A, 38, 1
Sneden, C., & Parthasarathy, M. 1983, ApJ, 267, 757
Sneden, C., Preston, G. W., McWilliam, A., & Searle, L. 1994, ApJ, 431, L27
Spite, F., & Spite, M. 1993, A&A, 279, L9
Thévenin, F. 1989, A&AS, 77, 137
Thorburn, J. A., & Beers, T. C. 1992, BAAS, 24, 1278
Timmes, F. X., Woosley, S. E., & Weaver, T. A. 1995, ApJS, 98, 617
Truran, J. W. 1981, A&A, 97, 391
Unsöld, A. 1955, Physik der Sternatmosphären (2d ed.; Berlin: Springer)
van Winckel, H., Waelkens, C., & Waters, L. B. F. M. 1995, A&A, 293, L25
Waines, H., & Schacht, S. 1978, Psychometrika, 43, 203
Wheeler, J. C., Sneden, C., & Truran, J. W., Jr. 1989, ARA&A, 27, 279
White, H. E., & Eliason, A. Y. 1933, Phys. Rev., 44, 753
Woosley, S. E. 1982, in Bessell & Norris (1984), n.2
Woosley, S. E., & Hoffman, R. D. 1992, ApJ, 395, 202
Woosley, S. E., & Weaver, T. A. 1986, ARA&A, 24, 205
———. 1995, ApJS, 101, 181
Woosley, S. E., Wilson, J. R., Mathews, G. J., Hoffman, R. D., & Meyer, B. S. 1994, ApJ, 433, 229
Zhao, G., & Magain, P. 1990, A&A, 238, 242